Miner Deposita (2006) 41: 483–503
DOI 10.1007/s00126-006-0074-6

ARTICLE

Napoleon Q. Hammond · John M. Moore

Archaean lode gold mineralisation in banded iron formation at the Kalahari Goldridge deposit, Kraaipan Greenstone Belt, South Africa

Received: 1 June 2005 / Accepted: 29 May 2006 / Published online: 12 July 2006

Abstract The Kalahari Goldridge Mine is located within the Archaean Kraaipan Greenstone Belt, about 60 km southwest of Mafikeng in the North West Province, South Africa. The ore body thickness varies from 15 to 45 m along a strike length of about 1.5 km within approximately N–S striking banded iron formation (BIF). The stratabound ore body is hosted primarily by BIF, which consists of alternating chert and magnetite–chlorite–stilpnomelane–sulphide–carbonate bands of millimetre- to centimetre scale. A footwall of sericite–carbonate–chlorite schist underlain by mafic amphibolite occurs to the west and carbonaceous metapelites in the hanging wall to the east. Overlying the hanging wall, carbonaceous metapelites, units of coarse-grained metagreywackes fining upwards, become increasingly conglomeratic up the stratigraphy. Small-scale isoclinal folds, brecciation, extension fractures and boudinage of cherty BIF units reflect brittle-ductile deformation. Fold axial planes have foliation, with subvertical plunges parallel to prominent rodding and mineral lineation in the footwall rocks. Gold mineralisation is associated with two generations of quartz–carbonate veins, dipping approximately 20° to 40° W. The first generation consists of ladder-vein sets (group IIA) preferentially developed in centimetre-scale Fe-rich meso-bands, whereas the second generation consists of large quartz–carbonate veins (group IIB), which locally crosscut the entire ore body and extend into the footwall and hanging wall. The ore body is controlled by mesoscale isoclinal folds approximately 67° E, orthogonal to the plane of mineralised, gently dipping veins, defining the principal stretching direction and development of fluid-focussing conduits. The intersections of the mineralised veins and foliation planes of the host rock plunges approximately 08° to the north. Pervasive hydrothermal alteration is characterised by chloritisation, carbonatisation, sulphidation and K-metasomatism. Gold is closely associated with sulphides, mainly pyrite and pyrrhotite, and to a lesser extent, with bismuth tellurides and carbonate minerals. Mass balance transfer calculations indicate that hydrothermal alteration of BIF involved enrichment of Au, Ag, Bi, Te, S and CO_2 (LOI), MgO, Ba, K and Rb, but significant depletion of SiO_2 and, to a lesser extent, Fe_2O_3. Extensive replacement of magnetite and chlorite in BIF and other pelitic sedimentary rocks by sulphide and carbonate minerals, both on mesoscopic and microscopic scales, is evidence of interaction of CO_2- and H_2S-bearing fluids with the Fe-rich host rocks. The fineness of gold grains ranges from 823 to 921, similar to that of other epigenetic Archaean BIF-hosted gold deposits, worldwide.

Keywords Archaean · Kraaipan greenstone belt · Banded iron formation · Gold · South Africa

Editorial handling: H. Frimmel

N. Q. Hammond · J. M. Moore
Department of Geology, Rhodes University,
Grahamstown 6140, South Africa

Present address:
N. Q. Hammond (✉)
Geological Survey of Japan, AIST Tsukuba,
Central 7, Higashi 1-1-1,
Tsukuba 305-8567, Japan
e-mail: quaye.hammond@msn.com

Introduction

The Kaapvaal Craton in South Africa (Fig. 1) is host to many of the country's mineral resources, including the famous Witwatersrand gold and Bushveld platinum and chrome deposits. In addition, the craton contains several Archaean greenstone belts, including the well-known Barberton and Murchison belts. The Kalahari Goldridge gold deposit, however, is sited in the Kraaipan greenstone belt, which has received relatively little geological attention compared to the Murchison and Barberton greenstone belts, due to poor exposure, lack of geochronological data and relatively few known mineral deposits of any significance. However, the development of the Kalahari Goldridge gold mine in the 1990s has assisted in a greater understanding of the geology and hydrothermal activity in the greenstone belt. The Kalahari Goldridge deposit com-

prises four discrete ore bodies (D Zone, A Zone, Watertank and Windmill), hosted in banded iron formation (BIF), with the D Zone, which is the focus of this study, being the largest of the deposits. In 1996, mining operations began at the D-Zone deposit with an average gold grade of 2.4 g/t and a subsequent annual production of 80,000 oz of gold.

This study examines gold mineralisation at the Kalahari Goldridge deposit and its relationship to hydrothermal alteration, which, together with field relationships, provide a framework for understanding the timing and controls of the BIF-hosted mineralisation. Within the spectrum of epigenetic BIF-hosted gold deposits, Kalahari Goldridge deposit is somewhat unusual in that it represents a deposit formed during low-PT conditions and relatively brittle deformation.

Geological setting

Regional geological setting

The Kraaipan greenstone belt is located in the North West Province of South Africa, in the west-central part of the Kaapvaal Craton (Fig. 1). Late Archaean volcanic rocks of the Ventersdorp Supergroup and Tertiary sedimentary rocks of the Kalahari Group cover a significant portion of the belt.

Several investigations (Zimmermann and Anhaeusser 1991; Jones and Anhaeusser 1993; Anhaeusser and Walraven 1999), aided by drill-hole intersections and airborne geophysical surveys, indicate that the Kraaipan Greenstone Belt extends discontinuously for approximately 250 km north-south from southern Botswana to Christiana (Fig. 2). While lack of exposure has made establishment of a complete regional stratigraphic succession for the greenstone belt difficult, subdivisions of the Kraaipan Group have been proposed on the basis of exposures of BIF and chert (SACS 1980).

In the north, the greenstones consist of three narrow NNW-striking belts (Stella, Kraaipan, Madibe) dominated by mafic metavolcanic rocks interlayered with ferruginous and siliceous metasedimentary rocks, mainly BIF and ferruginous chert. Model Pb–Pb isotope ages for the BIF indicate a minimum age of 3,400 Ma (Anhaeusser and Walraven 1999), while U–Pb zircon dating of plutonic rocks containing Kraaipan greenstone xenoliths confirms

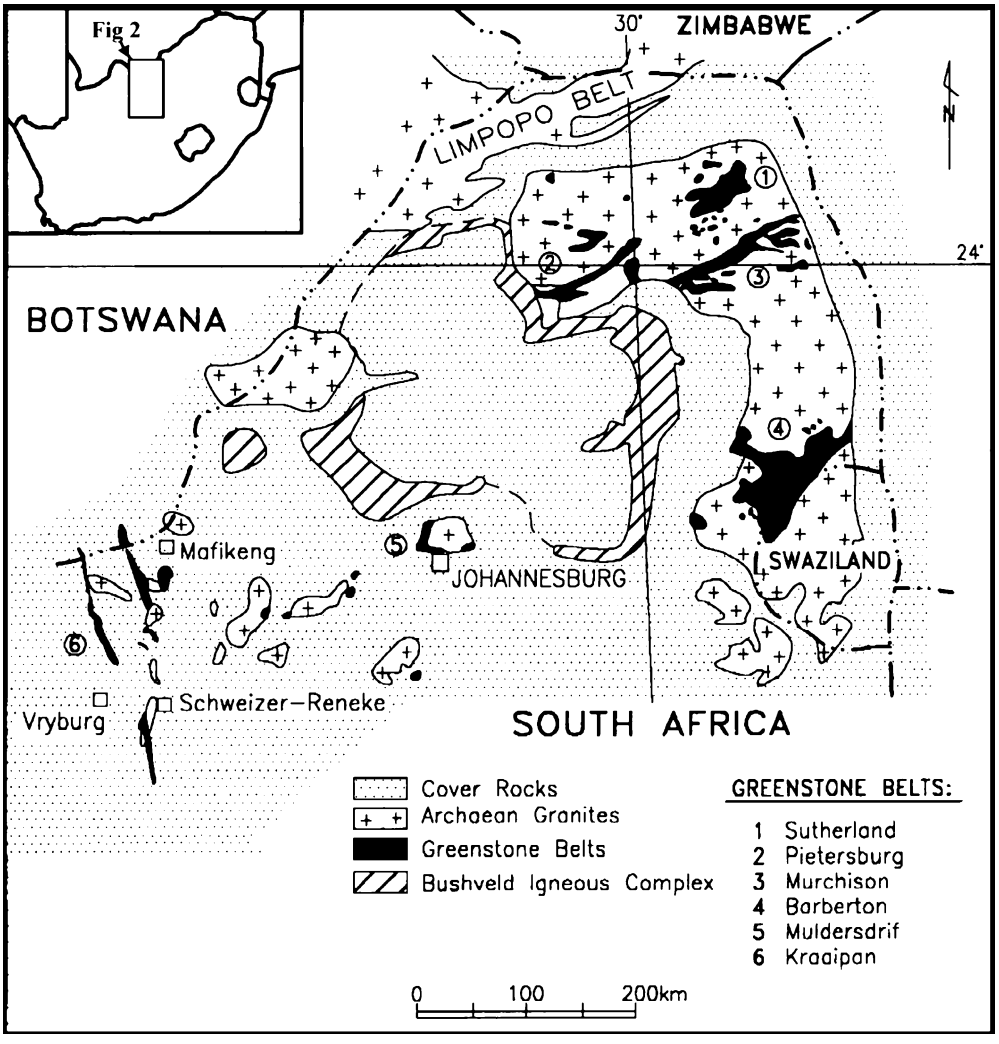

Fig. 1 Simplified geological map of the Kaapvaal Craton, South Africa, showing the distribution of Archaean basement rocks and greenstone terranes (after Anhaeusser and Walraven 1999)

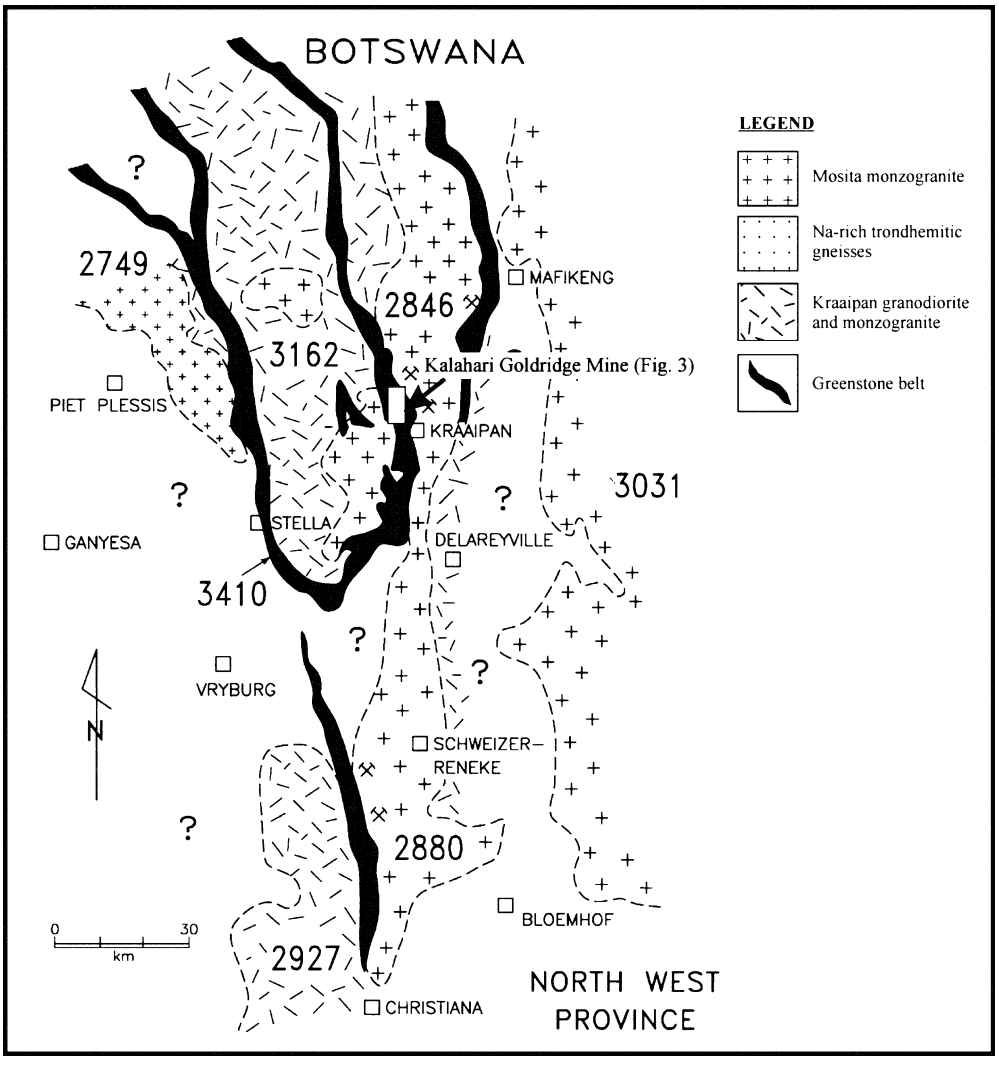

Fig. 2 Simplified geological map of the Kraaipan granite–greenstone terrane (after Anhaeusser and Walraven 1999). Map is largely based on combined aeromagnetic and gravity interpretation due to limited exposure

that the latter are older than 3,010 Ma (Poujol et al. 2002). Based on amphibole–chlorite–epidote assemblages in metavolcanic rocks, Anhaeusser and Walraven (1999) deduced that lower greenschist to amphibolite facies metamorphism had affected the belt.

Kraaipan plutonic rocks

The Kraaipan Greenstone Belt has been intruded by a variety of granitoids, classified by Zimmerman and Anhaeusser (1991) into three groups based on field relationships, petrology, geochemistry and geochronological constraints. These are a tonalitic–trondhjemitic gneiss–migmatite suite (TTG), a granodiorite–monzogranite suite and the Mosita monzogranite. The TTG suite, which has extensive sub-outcrop in the western Kaapvaal Craton, has yielded zircon Pb-evaporation dates from 3,070 to 3,162 Ma (Anhaeusser and Walraven 1999) and conventional U–Pb zircon ages of 3,008±4 Ma (Poujol et al. 2002). Zircon Pb-evaporation dates (Anhaeusser and Walraven 1999) and conventional U–Pb dates (Poujol et al. 2002) indicate ages of 2,846±22 and 2,879±11 Ma, respectively, for the granodiorite–monzogranite suite, which has a more restricted distribution than the TTG suite, occurring primarily in a north–south trending zone along the eastern margin of the Kraaipan and Amalia greenstone belts (Anhaeusser and Walraven 1999). The Mosita monzogranite, which has U–Pb zircon ages of 2,718±65 and 2,790±8 Ma (Burger and Walraven 1979; Poujol et al. 2002, respectively) and a zircon evaporation age of 2,749±3 Ma (Anhaeusser and Walraven 1999), is the youngest granitic intrusion in the Kraaipan Greenstone Belt. The monzogranite is mostly buried beneath Tertiary Kalahari cover, but has been reported from drill-hole intersections along the northwestern margins of the greenstone belt at Stella.

Anhaeusser and Walraven (1999) and Poujol et al. (2002) proposed that the Kraaipan volcano-sedimentary greenstone belt and associated granitoids evolved as a result of episodic accretion of juvenile crust on to the western boundary of the Kaapvaal Craton between ca. 3,010 and 2,790 Ma.

Host sequence lithostratigraphy

The Kalahari Goldridge deposit, located about 60 km southwest of Mafikeng, contains mafic schist in the footwall to the ore-hosting BIF horizon and a succession of clastic metasedimentary rocks, consisting of carbonaceous phyllite, schist and greywacke, in the hanging wall (Fig. 3). A series of steeply dipping post-mineralisation dolerite dykes up to 1 m thick, intrude the ore body.

Mafic schist

This unit, which forms the footwall to the ore body, consists of metabasaltic rocks (Anhaeusser and Walraven 1999) comprising actinolite and lesser amounts of epidote, quartz, calcite and plagioclase. The immediate footwall unit is a strongly bleached and altered mafic schist with loss of original basaltic texture, consisting essentially of calcite, sericite and quartz with minor chlorite. Further from the ore body, the basaltic protolith is better preserved and contains primary textures such as pillow lavas with amygdales.

Banded iron formation (BIF)

The BIF, which hosts the D-Zone ore body, varies from about 15 to 45 m thick along a strike length of 1.5 km. It forms a competent unit in the central part of the deposit but grades at the margins into banded ferruginous chert interbedded with chloritic schist. The BIF consists of alternating chert and magnetite bands ranging from submillimetre (microbands) to centimetre scale (mesobands) in thickness. Rare least-altered BIF units contain mainly magnetite and quartz with limited replacement of magnetite by minor stilpnomelane and siderite.

Stilpnomelane and chlorite are the dominant Fe-silicate phases in altered BIF. Stilpnomelane exhibits a range of habits and varies from pale green to brown and reddish-brown (Fig. 4a–f). Textural relationships between stilpnomelane and coexisting minerals in altered rocks indicate that it developed from ore–fluid reaction with Fe-rich rocks. The dominant brown variety exhibits an interlocking acicular or lath-like habit and is intimately associated with fine-grained carbonate minerals, both of which have replaced green stilpnomelane sheaves or chlorites (Fig. 4b). Green stilpnomelane occurs in some least-altered BIF samples as fine-grained laths intergrown with minnesotaite in magnetite microbands. In more altered chert-magnetite and magnetite BIF mesobands, coarse-grained acicular aggregates, sheaves and rosettes of stilpnomelane are intergrown with sulphides. Minnesotaite also occurs as colourless grains associated with quartz, siderite and pyrite-pyrrhotite in individual magnetite-rich microbands of chert-magnetite mesobands in some least-altered BIFs and shows clear evidence of formation from reactions between siderite and quartz, and pyrrhotite and quartz (Fig. 4e).

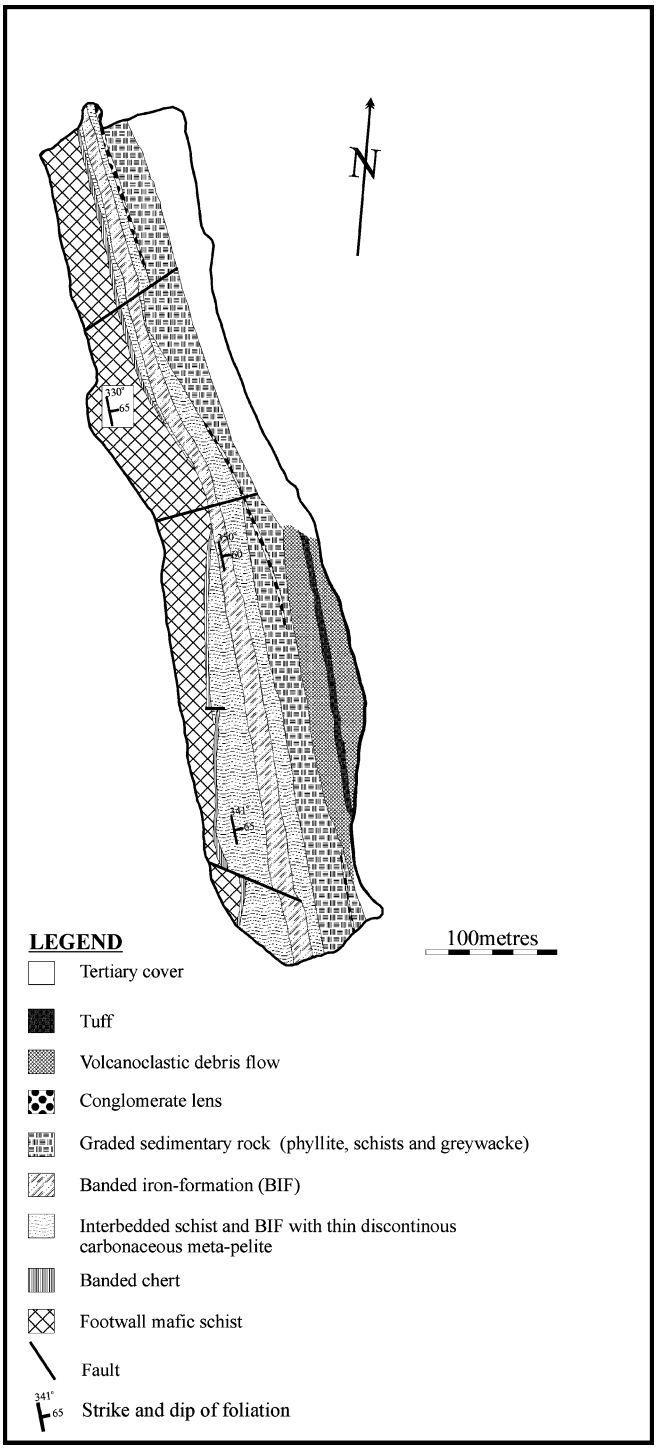

Fig. 3 Simplified geological map of the D-Zone open pit at the Kalahari Goldridge deposit (as of August 2000). Information on the geology of the deposit has been derived mainly from drill-hole intersections, exposures in the open-pit operations and rare outcrops outside of the mine area

Coarse-grained olive-green chlorite occurs as tabular to equi-granular grains intergrown with recrystallised magnetite and other alteration minerals in altered BIF. Muscovite is a minor phase in the quartz veins and BIF, and occurs as flaky or tabular coarse grains. Carbonate minerals in the

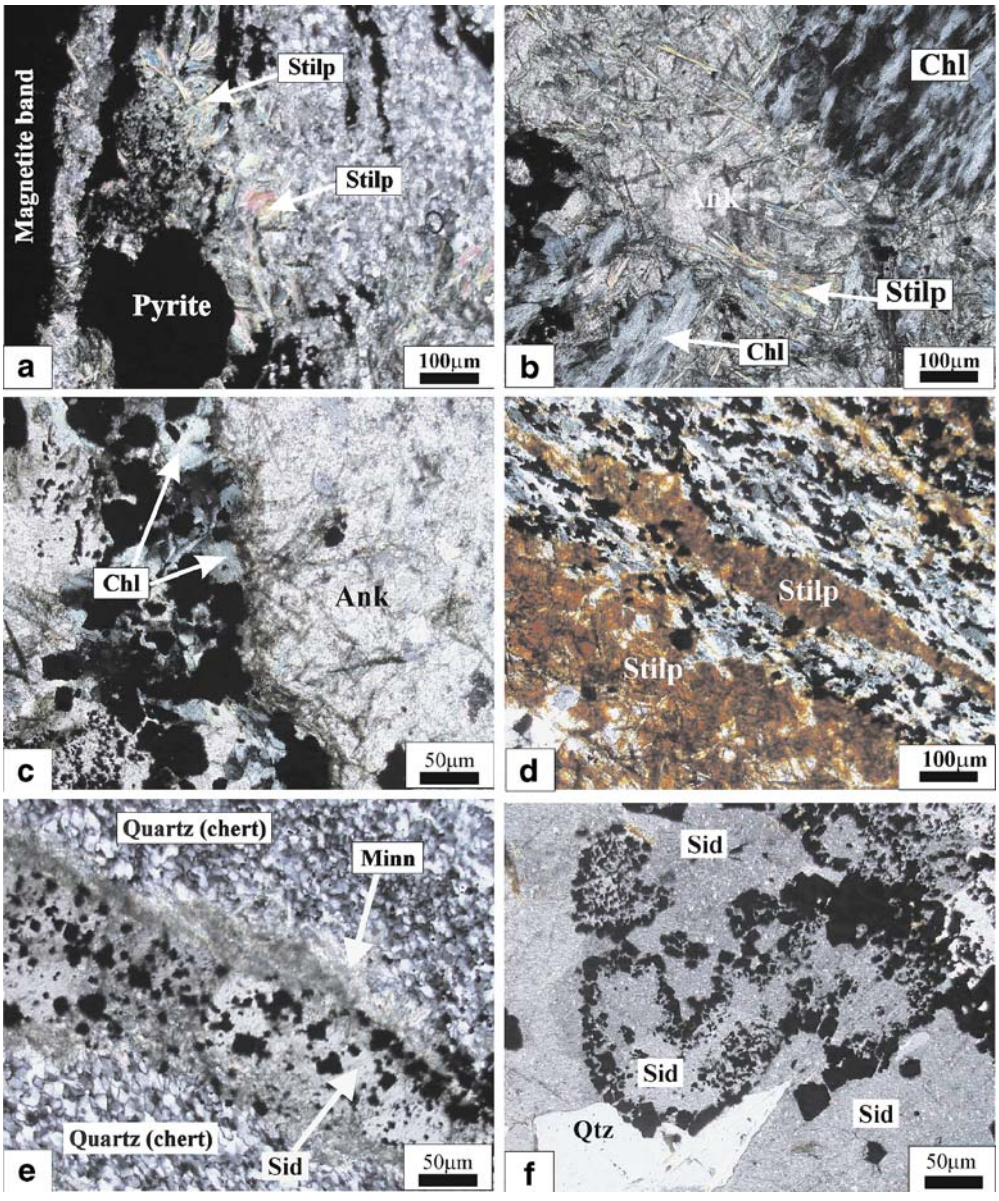

Fig. 4 Photomicrographs of replacement textures at the Kalahari Goldridge deposit: **a** Ferrostilpnomelane (Stilp), which has replaced magnetite along a less altered magnetite microband; **b** truncation of chlorite band (*Chl*) by ferrostilpnomelane (*Stilp*) and ankerite (*Ank*) in interbedded schist; **c** ferristilpnomelane, which has replaced chlorites (*Chl*) along grain boundaries in altered BIF; **d** ferristilpnomelane (*Stilp*), which has replaced chlorite band. Dispersed opaque grains are magnetite grains, which have been partially replaced by pyrite and pyrrhotite; **e** photomicrograph showing development of minnesotaite (acicular grains, Minn) along siderite–quartz boundary in least altered BIF; **f** magnetite (opaque grains) replacement by siderite (*Sid*) in BIF. All photos were taken in crossed polarised light

BIF and vein selvedges are dominated by siderite with minor amounts of ankerite. In least-altered and less-deformed BIF, siderite occurs in thin but continuous microbands as a replacement product after magnetite in magnetite mesobands. In altered samples, siderite occurs mostly as coarse anhedral to euhedral grains or as massive aggregates, mainly as partial to complete pseudomorphic replacements of magnetite (Fig. 4f), sulphide minerals or chlorite.

Magnetite occurs as small octahedral grains in least-altered BIF, generally along monomineralic layers and as disseminations or as coarse-grained euhedral crystals where significant recrystallisation has occurred.

Coexisting pyrite and pyrrhotite normally exhibit annealing textures and, hence, show no clear paragenetic order. However, small inclusions of pyrrhotite, in places with gangue minerals and/or visible gold, in pyrite suggest that pyrrhotite generally preceded pyrite in the crystallisation sequence. Pyrite in altered BIF is commonly intergrown with stilpnomelane, chlorite or siderite, providing evidence of their contemporaneous growth. Pyrite also occurs as coarse subhedral to euhedral grains, having replaced both magnetite in the BIF and chlorite along foliation planes in the interlayered schist, where there are inclusions of gangue minerals in the cores of pyrite grains.

Footwall and hanging wall schist/chert association

Metasedimentary rocks, gradational between mica schist and chert, are interlayered with ferruginous chert and separate the centrally located massive BIF from the footwall and hanging wall rocks. They form thin lenses, generally less than 1 m thick of chlorite-rich bands locally alternating with centimetre-scale magnetite-rich and cherty bands. Thin graphite- and pyrite-bearing metapelites,

ranging from 1 to 2 m in thickness, occur discontinuously at the contacts of the BIF horizon with footwall mafic schist and the hanging wall clastic metasedimentary units. The metapelites typically contain stringers of carbonaceous material that anastomose around quartz and carbonate augen.

Chlorite, stilpnomelane, sericite, carbonate and quartz are the main constituents of the metapelites with magnetite, pyrite and pyrrhotite occurring locally in significant proportions (40–50%). In the interlayered schist, chlorite typically occurs as green schistose or felt-like masses. In altered schist, characterised by microfractures and centimetre-scale ladder veins, however, pale-blue Fe-rich chlorite exhibits medium- to coarse-grained mosaic textures, occurring as sheaves, rosettes or interlocking acicular grains. Muscovite typically replaced chlorite and is best developed in the interbedded schists within the ore body. Magnetite occurs as disseminated grains in a chlorite matrix. Pyrrhotite replacement of chlorite occurs locally, associated with dark brown stilpnomelane, carbonate and pyrite. Pyrite occurs as subhedral to euhedral grains in bands or semi-discrete layers subparallel to foliation planes in interlayered schist or as replacement of chlorite along foliation planes.

Hanging wall metasedimentary rocks

The immediate hanging wall comprises a succession of metapelites and meta-greywackes, consisting of metre-scale fining-upward cycles that generally coarsen up-sequence. Graded Bouma-cycle units commence with a conglomerate followed by greywacke and terminate with a phyllitic cap. Conglomerate clasts are dominated by chert fragments at the base of the sequence, with amphibolite and lesser BIF clasts becoming progressively more common up-sequence, indicating a local source. Mafic clasts reach 30 cm in diameter at the top of the intersected stratigraphy where coarse debris flows dominate over finer units. The hanging wall succession has the characteristics of a rapidly prograding submarine fan sequence.

Structure

Structural elements at the Kalahari Goldridge deposit are dominated by the uniform regional foliation of the greenstone belt, which has an average orientation of 340° and a dip of 67° E (Fig. 5a). The earliest tectonic fabric developed in the area is a bedding-parallel foliation defined by aligned phyllosilicate and carbonate grains, which is best developed in the footwall schists and phyllites.

Mineral lineations are defined by elongate quartz and sulphide grains in the schistose units, strained clasts in the conglomeratic units in the hanging wall and rods in BIF. The mineral lineations have an average plunge of 67° towards 108° (Fig. 5a). Small-scale isoclinal folds are common in the schist and BIF, and have axial planes (average 334°/61° E) subparallel to foliation. This is interpreted to be the result of rotation of the fold axes into parallelism with foliation during shearing. The axes of the isoclinal folds are subparallel to the mineral lineations.

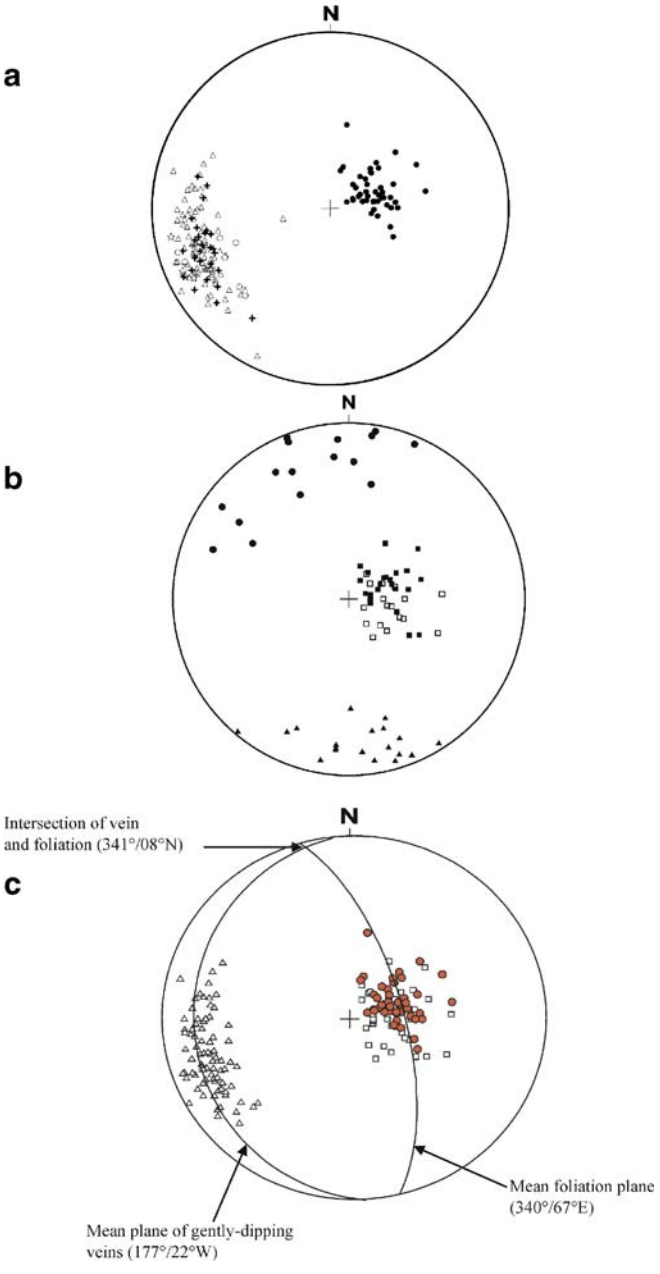

Fig. 5 **a** Lower hemisphere projection of major structural elements. Poles to bedding plane (*crosses*), poles to foliation plane (*triangles*), poles to axial plane of isoclinal fold (*circles*), poles to shear plane (*stars*) and mineral lineations (*filled circles*). **b** Quartz–carbonate vein orientation at the Kalahari Goldridge deposit. Group I (*filled circles*), group IIA (*open squares*), group IIB (*filled squares*) and group III veins (*filled triangles*). **c** Major structures controlling mineralisation at the Kalahari Goldridge deposit. The primary control is illustrated by the orthogonal orientation of the mineral elongation lineations (*filled circles*) to the gently dipping (group II) veins. A secondary predicted control is the intersection of the planes of the foliation and the gently dipping veins at approximately 341°/08° N. Legend: *triangles* poles to foliation plane, *squares* poles to plane of mineralised veins, *filled circles* mineral elongation lineations

Large open folds extend along the entire length of the ore body in a north–south direction, with subvertical axial planes and fold axes plunging steeply to the east. Centimetre-scale boudins are developed in some mineralised cherty BIF bands, which host gently dipping extension veins. The boudins, defined by orthogonal fracturing of Fe-rich and siliceous bands, are commonly filled with quartz±carbonates. The boudins are more commonly developed in magnetite-rich mesobands than in adjacent siliceous mesobands. Large-scale boudins also occur where the interbedded chlorite schist wraps around large BIF blocks, forming anastomosing networks of boudins. Variable degrees of development of the boudins indicate that deformation was progressive, with the initial development of necking followed by extension fractures and vein formation.

Vein systems and geometry

Mapping in the open pit at Kalahari Goldridge has identified three broad groups of quartz veins (groups I, II, III) that are defined on the basis of structural orientation, mineralogy and crosscutting relationships (Fig. 5b).

Group I veins are steeply dipping and oriented approximately at 064°/74° S. They have a simple mineralogy dominated by ankerite and dolomite (90–95%) with variable amounts of quartz. The carbonates form lenses extending several centimetres in length, but less than 5 cm in width. They are commonly buckled and distorted, and exhibit *en echelon* sigmoidal forms in places. Group I veins are cut by groups II and III and predate the gold mineralisation.

Group II veins (Fig. 6) are dominant at the Kalahari Goldridge mine and are closely associated with gold mineralisation. They consist of ankerite, siderite, quartz, pyrite and pyrrhotite with minor chalcopyrite, ferristilpnomelane and chlorite. Pale green chlorite occurs as sheaves, rosettes or felt-like equi-granular aggregates, intergrown with carbonate and quartz in a mosaic texture. The veins crosscut the regional foliation at a steep angle, with average strike of about 174° and dips ranging from about 10 to 40° W. The adjacent wall rocks display minimal or no evidence of displacement across the veins.

Group II veins are further subdivided into earlier group IIA and later group IIB veins. The group IIA veins are best developed in BIF, are preferentially developed in Fe-rich bands, and exhibit regular spacing sub-perpendicular to layering in a ladder array (Fig. 6a–c). Their thickness ranges from a few millimetres to 2 cm and their lateral extent is generally defined by the width of the Fe-rich band, but typically up to 5 cm. The group IIB veins (Fig. 6a), on the other hand, are massive, with thickness up to 20 cm, and extend laterally in excess of 20 m through the entire ore body and, in places, into the hanging wall and footwall. Carbonate selvedges along the contact between the host BIF and vein are common. Sulphide-bearing haloes are also common at the contacts extending up to several centimetres into the host BIF.

The youngest group III veins, with an average orientation of 266°/74° N, consist of ankerite-dolomite and quartz. The veins have uniform thickness, up to about 10 cm, and a lateral extent of several metres. Thin pyrite laminations along selvedges with the host rocks are a prominent characteristic. These veins show no association with gold mineralisation.

Deformation history

At least three phases of deformation are recorded, (D_1 to D_3). The early regional deformation D_1, is synchronous with low-grade regional metamorphism of the greenstone units. A penetrative NNW–SSE trending schistosity, which developed subparallel to the primary lithological layering characterises this event. D_2 deformation was largely ductile and accompanied by crustal shortening, resulting in tight isoclinal folding, boudinage and shearing within the BIF. The D_2 deformation progressed to more brittle deformation, characterised by extensional fractures in more competent and Fe-rich BIF in which the group II veins developed. The D_2 event is inferred to have reoriented the axial planes of tight-to-isoclinal folds into parallelism with the S_1 foliation. D_2 is also characterised by NNW–SSE shortening as shown by buckling of the earliest-formed group I (metamorphic) quartz-carbonate veins. D_3 is associated with flexuring of the major N–S belt and development of broad open folds with easterly plunging subvertical fold axes. The consistency of bedding and foliation planes in the deposit suggests that at the Kalahari Goldridge Mine, the D_2 and D_3 deformational events did not cause major changes in the structural geometry produced during D_1.

Hydrothermal alteration

Alteration of host rocks at the Kalahari Goldridge deposit is pervasive, extending into the footwall and hanging wall. It has overprinted the regional metamorphic assemblage and generally makes it impossible to define unaltered rock types hosting the ore body in the deposit.

Potassium metasomatism, sulphidation, carbonitisation and chloritisation are the main processes associated with a hydrothermal alteration pattern, which reflects in part the distribution and composition of the host rocks, but overall, is consistent throughout the deposit. Potassium metasomatism forms white mica and stilpnomelane, which occur mainly in the ore zone. The degree of alteration is apparently controlled by the degree of group II ladder veining. In the ore zone, the modal abundances of ankerite and siderite correspond closely to the intensity of alteration and the density of veining. In the footwall and hanging wall schists, bleaching is most intense in areas proximal to the ore body. Calcite alteration is restricted to the footwall, and to a lesser extent, to the hanging wall and may be attributed to the breakdown of epidote and plagioclase, which are common in less-altered mafic schists.

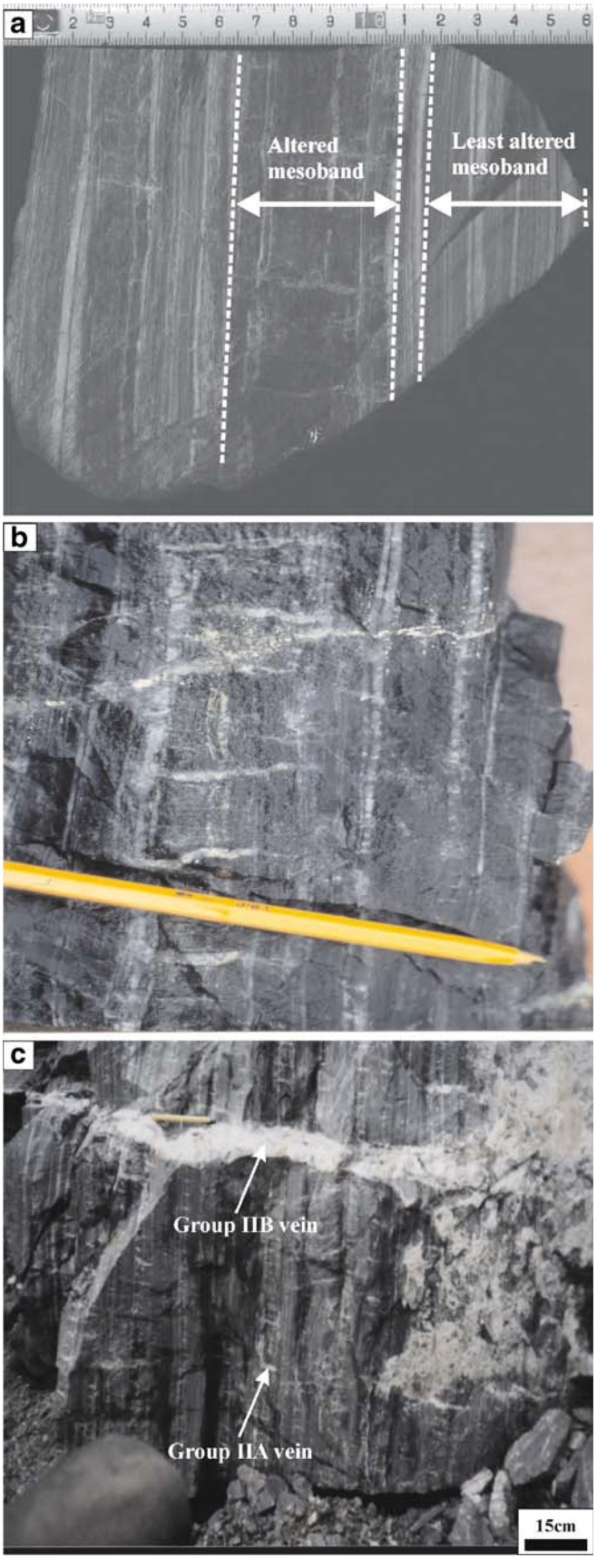

◀ **Fig. 6** Photographs showing the mineralised (group II) quartz–carbonate veins in BIF at the Kalahari Goldridge deposit. Group IIA vein (**a**–**c**) preferentially developed in BIF mesobands, and group IIB (**c**) vein cutting through entire BIF. Also, shown in **a** is least-altered mesoband

Gold mineralisation and hydrothermal alteration at the Kalahari Goldridge deposit are both largely associated with lithological variation. Most gold is concentrated in zones of intense carbonate–sulphide–chlorite alteration confined to the central part of the BIF, within the Fe-rich section of the ore body. A large proportion of the gently dipping group IIA ladder veins are also confined to the BIF units. Centimetre-scale sulphidation haloes are also associated with the large gently dipping group IIB veins mainly within the BIF.

Mineral chemistry

Table 1 lists the mineral assemblages in various rock types at the Kalahari Goldridge deposit. Compositions of minerals were acquired by wavelength dispersive spectrometry (WDS) and energy dispersive spectrometry (EDS) on carbon-coated polished thin sections and briquettes, using a Jeol CXA-733 Superprobe in the Department of Geology at Rhodes University. Analyses of carbonate minerals were performed using EDS at 15 kV operating voltage and 20 nA beam current with 100 s counting time. The silicate minerals were analysed by WDS at 15 kV operating voltage and 20 nA beam current, whereas electrum and ore minerals were analysed at 20 kV and 30 nA with counting times maintained at 20 s for all elements. Calibrations were done using international standards, and the analyses were corrected using ZAF correction.

Based on the classification of Hey (1954), chlorite is mainly ripidolite in composition (Table 2) with a few analyses of group IIB vein chlorites showing compositions characteristic of pycnochlorite. Fe/(Fe+Mg) ratios, however, are significantly variable, ranging from 0.65 to 0.79 (average 0.71) for chlorite in the interlayered schist, through 0.76 to 0.85 (average 0. 81) for chlorite in the BIF, to 0.69 to 0.77 (average 0.73) for chlorite in IIA veins, and 0.57 to 0.76 (average 0.66) for the IIB veins.

The composition of stilpnomelane shows a wide range of Al_2O_3 from 4.76 to 9.6 wt% (Table 3). Total Fe as FeO in the stilpnomelane ranges from 32.13 to 32.5 wt% and bears no relationship to host-rock composition. The K_2O contents in stilpnomelane are highly variable-dependent on the degree of oxidation, ranging from about 1.0 wt% in the reddish-brown stilpnomelane to about 3.4 wt% in the green variety. Microprobe analyses show that the muscovite is phengitic in composition.

Thirty siderite and 24 ankerite grains in veins, BIF and interbedded schist, exhibit some compositional variations (Fig. 7a). Group IIA vein siderite ($Fe_{0.64}Mg_{0.31}Mn_{0.03}Ca_{0.02}CO_3$) exhibits more Fe-enrichment than group IIB vein siderite, ($Fe_{0.56}Mg_{0.33}Mn_{0.09}Ca_{0.02}CO_3$). Average

Table 1 Modal abundance of minerals at the Kalahari Goldridge deposit

	Hanging wall			Ore body				Footwall
	Greywacke	Schist	Phyllite	BIF	Interbedded schist	Group IIA veins	Group IIB veins	Mafic schist
Mineral oxide								
Magnetite	–	–	–	xxxx	xx	x	x	–
Ilmenite	–	x	–	–	xx	–	–	x
Sulphide								
Pyrite	x	xx	xx	xxxx	xx	xx	xx	x
Pyrrhotite	–	x	x	xxxx	xx			x
Chalcopyrite	–	–	–	xx	xx	x	x	–
Silicate								
Quartz	xxxx	xxx	xxx	xxxx	xxxx	xxxx	xxxx	xxx
Chlorite	xxx	xxxx	xxx	xxx	xxxx	xx	xx	xxx
Stilpnomelane	–	–	–	xxxx	xxx	xx	xx	–
Muscovite	xxx	xxx	xxx	x	xxxx	x	x	xxx
Minnesotaite	–	–	–	x	x	–	–	–
Plagioclase	–	–	–	–	–	–	–	x
Epidote	–	–	–	–	–	–	–	x
Actinolite	–	–	–	–	–	–	–	x
Carbonate								
Siderite	–	–	–	xxxx	–	xx	xx	–
Ankerite-dolomite	x	xxx	xxx	xx	xxx	xxx	xxx	xx
Calcite	x	xx	x	–	–	–	–	xxx
Bismuth minerals								
Native bismuth	–	–	–	x	–	–	–	–
Bismuth telluride	–	–	–	x	–	–	–	–
Gold	–	–	–	xx	x	x	x	–

xxxx = abundant (>60 modal %); xxx = common (20–60 modal %); xx = less common (5–20 modal %); x = rare (<5 modal %); – =not found

siderite composition in altered BIF ($Fe_{0.76}Mg_{0.19}Mn_{0.05}Ca_{0.01}CO_3$) shows marked enrichment in Fe relative to Mg, compared to that in least-altered BIF ($Fe_{0.56}Mg_{0.33}Mn_{0.09}Ca_{0.02}CO_3$). Similarly, ankerite compositions from three schist samples indicate a significant compositional variation in Mg, Fe and Mn, from $CaMg_{0.33}Fe_{0.57}Mn_{0.10}(CO_3)_2$ in least-altered schist to $CaMg_{0.73}Fe_{0.27}(CO_3)_2$ in the most altered sample. These variations indicate extensive Fe exchange for Mg with increasing alteration.

Microprobe analyses reveal that magnetite contains less than 2 wt% in total of MgO, Al_2O_3, TiO_2, Cr_2O_3 and MnO. Bismuth telluride group minerals are rarely associated with pyrrhotite and/or gold along grain boundaries. Native bismuth is exsolved along grain boundaries or occurs as inclusions in pyrrhotite. Microprobe analyses of Bi minerals (Fig. 7b) indicate compositions ranging from native Bi to Bi-telluride minerals in the tetradymite series, which are stable at temperatures ranging from 200 to 400°C (Marcoux et al. 1996). There are minor amounts of Fe (up to 1.67 wt%) in all analysed grains (Table 4). The lack of sulphur in these minerals and their close association with pyrrhotite suggests that deposition occurred under conditions of relatively low sulphur activity. Gold occurs as isolated grains or closely associated with sulphide and gangue minerals, notably carbonates, mainly in altered BIF. Gold associated with sulphide commonly occurs as inclusions in pyrite (Fig. 8a), as blebs or coarse grains along boundaries of pyrrhotite, pyrite and gangue minerals (Fig. 8d), as microcrack fillings in pyrite (Fig. 8d), or as discrete grains (Fig. 8c). The grain size of the subrounded to angular gold is highly variable from less than 1 to 100 μm in diameter. Nearly 80% of visible gold is associated with pyrite grains that have replaced magnetite. There are high Au assay values in pyrrhotite-rich samples, but visible gold is rare, suggesting that some gold is present at submicroscopic levels or in lattice sites of pyrrhotite.

Microprobe analyses of 14 gold grains indicate only trace amounts of Fe, Cu and S. Minor amounts of Ag-rich gold have been found associated with bismuth minerals. Fineness of the gold grains [1,000*Au/(Au+Ag)] ranges from 823 to 931, with the lowest values (823–830) associated with bismuth tellurides (Table 4).

Mineral paragenesis

The paragenetic sequence of the mineral assemblages at Kalahari Goldridge is divided into pre-ore, main stage and post-gold mineralisation (Fig. 9). Minerals associated with the pre-ore stage are identified in least-altered BIF and schist. They include magnetite, quartz (chert), minnesotaite and siderite in the BIF, and chlorite, actinolite, plagioclase,

Table 2 Average microprobe analyses of chlorite in various rock types at the Kalahari Goldridge deposit

Sample no.	Interbedded schist		Mineralised BIF		Group IIA veins		Group IIB veins	
No. of analyses	Mean 28	SD	Mean 30	SD	Mean 21	SD	Mean 24	SD
SiO_2	24.02	1.01	22.74	0.53	24.33	0.88	24.26	0.97
TiO_2	0.07	0.01	0.06	0.02	0.04	0.01	0.06	0.01
Al_2O_3	21.01	0.34	19.87	0.46	19.71	0.50	20.11	0.92
FeO[a]	35.03	1.89	39.12	1.85	35.33	1.11	32.75	2.96
MnO	0.16	0.07	0.09	0.04	0.10	0.05	0.12	0.04
MgO	8.14	1.27	5.17	0.95	7.27	0.97	9.39	2.42
CaO	0.05	0.03	0.06	0.03	0.04	0.05	0.03	0.02
Na_2O	0.05	0.05	0.08	0.08	0.03	0.02	0.02	0.01
K_2O	0.03	0.02	0.04	0.03	0.02	0.04	0.00	0.01
Total	88.57	1.80	87.24	1.55	86.85	0.84	86.75	1.14
Cations per formula unit based on 14 oxygens								
Si	2.65	0.06	2.62	0.04	2.74	0.08	2.70	0.04
Al (iv)	1.35	0.06	1.38	0.04	1.26	0.08	1.30	0.04
Tetrahedral site	4.00	0.00	4.00	0.00	4.00	0.00	4.00	0.00
Al (vi)	1.38	0.05	1.33	0.03	1.37	0.05	1.35	0.06
Ti	0.01	0.00	0.00	0.00	0.00	0.00	0.01	0.00
Fe^{2+}	3.23	0.21	3.77	0.16	3.34	0.14	3.06	0.37
Mn	0.02	0.01	0.01	0.00	0.01	0.00	0.01	0.01
Mg	1.33	0.18	0.89	0.16	1.22	0.14	1.55	0.36
Octahedral site	5.97	0.05	6.00	0.03	5.95	0.07	5.97	0.02
Ca	0.01	0.00	0.01	0.00	0.00	0.01	0.00	0.00
Na	0.01	0.01	0.02	0.02	0.00	0.00	0.01	0.00
K	0.00	0.00	0.01	0.00	0.00	0.01	0.00	0.00
Totals	0.02	0.02	0.03	0.03	0.01	0.01	0.01	0.01
Fe/(Fe+Mg)	0.71	0.04	0.81	0.03	0.73	0.03	0.66	0.08

SD one standard deviation
[a]All Fe as FeO

epidote, pyrite and pyrrhotite in the schist. Early formed chlorite occurs throughout the pelitic schist in the ore body and hanging wall with trace amounts in the footwall. Actinolite, plagioclase and epidote in footwall mafic schist are regional metamorphic minerals.

The main stage represents the hydrothermal event and main episode of gold mineralisation as well as the formation of the bulk of the secondary silicate, carbonate and opaque minerals. This stage is characterised by brittle deformation, the subsequent introduction of the hydrothermal fluid and the equilibration with host rocks, which resulted in the formation of gold-bearing sulphide minerals (pyrite and pyrrhotite), bismuth minerals (native bismuth and bismuth tellurides), carbonate (siderite, ankerite) and silicate minerals such as white mica, stilpnomelane and chlorite. Recrystallised magnetite and quartz are also associated with this stage.

The main stage is further subdivided into substages A and B, which are associated with the mineralised quartz veins in the deposit. High proportions of pyrrhotite associated with group IIA veins and inclusions of pyrrhotite in pyrite indicate that pyrrhotite generally predates pyrite. The high proportion of pyrite associated with group IIB veins also indicates that stage B accounts for the majority of the pyrite. Textural relationships show that chlorite and stilpnomelane formed throughout the entire mineralisation stage. Native gold appears to be coeval with sulphides and other gangue minerals in both substages A and B.

The post-gold stage is characterised by late calcite and dolomite in veins and pyrite.

Whole-rock geochemistry of BIF

Forty-three BIF samples, consisting of five least-altered and 38 altered samples from the ore zone were analysed for major and trace elements. The least-altered samples are slabs of BIF mesobands characterised by fine, undeformed layering of chert and magnetite with no visible Group II ladder quartz veins. Their volatile content (LOI) is consistent with the minimal occurrence of hydrous silicates, carbonates and sulphides compared to altered equivalents. Major elements were analysed by X-ray fluorescence at Rhodes University and the University of the Witwatersrand, according to the procedure of Norrish and Hutton (1969). Trace elements, including Au, Ag, As, W, Sb and Te, were analysed by ICP-MS at the University of Cape Town, and have lower detection limits in the lower ppb range. Table 5 presents the average composition of these rocks.

Table 3 Microprobe data of stilpnomelane in various rock types in the ore body at the Kalahari Goldridge deposit

	Interbedded schist					Quartz vein			Mineralised BIF						
	1	2	3	4	5	6 Group IIB	7 Group IIB	8 Group IIB	9	10	11	12	13	14	15
No. of analyses	5	3	3	1	1	1	2	2	2	1	3	3	1	3	8
Colour of stilpnomelane	Green	Brown	Reddish brown	Brown	Brown	Brown	Dark brown	Dark brown	Brown	Brown	Pale brown	Green	Brown	Reddish Brown	Reddish Brown
SiO_2	46.66	45.02	43.92	44.97	46.62	41.41	45.10	45.57	45.79	49.91	43.70	46.77	47.81	46.81	47.65
TiO_2	0.00	0.01	0.00	0.01	0.02	0.09	0.01	0.00	0.01	0.00	0.02	0.01	0.00	0.00	0.04
Al_2O_3	5.03	6.51	7.28	6.74	6.64	8.30	4.90	5.02	5.55	6.46	5.35	5.45	5.50	6.38	7.11
FeO*	32.31	32.80	35.51	35.06	34.18	35.19	32.78	32.50	34.07	32.80	34.89	31.94	33.71	33.34	31.60
MnO	0.21	0.19	0.08	0.07	0.19	0.21	0.02	0.02	0.08	0.09	0.14	0.13	0.12	0.09	0.09
MgO	4.35	4.45	3.23	3.11	3.12	4.23	3.38	3.58	3.30	4.30	2.68	4.23	4.20	4.64	4.72
CaO	0.27	0.35	0.07	0.05	0.48	0.10	0.17	0.29	0.26	0.26	0.67	0.14	0.17	0.16	0.14
Na_2O	0.29	0.18	0.39	1.14	0.51	0.10	0.33	0.31	0.38	0.22	0.81	0.39	0.10	0.64	0.57
K_2O	2.98	1.87	1.64	2.07	1.97	1.69	1.16	0.99	1.56	1.84	3.22	3.41	1.55	1.09	1.15
Total	92.10	91.40	92.13	93.22	93.73	91.31	87.85	88.28	91.00	95.88	91.46	92.47	93.16	93.16	93.07
Cations per formula unit based on 11 oxygens															
Si	3.71	3.59	3.53	3.58	3.65	3.38	3.74	3.75	3.69	3.74	3.59	3.70	3.73	3.64	3.66
Al (iv)	0.29	0.41	0.47	0.42	0.35	0.62	0.26	0.25	0.31	0.26	0.41	0.30	0.27	0.36	0.34
Tetrahedral site	4.00	4.00	4.00	4.00	4.00	4.00	4.00	4.00	4.00	4.00	4.00	4.00	4.00	4.00	4.00
Al (vi)	0.18	0.21	0.22	0.21	0.26	0.18	0.22	0.23	0.22	0.31	0.11	0.21	0.24	0.23	0.31
Ti	0.00	0.00	0.00	0.00	0.00	0.01	0.00	0.00	0.00	0.00	0.00	0.00	0.00	0.00	0.00
Fe	2.15	2.20	2.39	2.33	2.24	2.40	2.27	2.23	2.30	2.06	2.40	2.11	2.20	2.17	2.04
Mn	0.01	0.01	0.01	0.00	0.01	0.01	0.00	0.00	0.01	0.01	0.01	0.01	0.01	0.01	0.01
Mg	0.52	0.53	0.39	0.37	0.36	0.51	0.42	0.44	0.40	0.48	0.33	0.50	0.49	0.54	0.54
Octahedral site	2.86	2.96	3.00	2.91	2.87	3.11	2.91	2.91	2.91	2.85	2.85	2.83	2.93	2.95	2.89
Ca	0.02	0.03	0.01	0.00	0.04	0.01	0.02	0.03	0.02	0.02	0.06	0.01	0.01	0.01	0.01
Na	0.05	0.03	0.06	0.18	0.08	0.02	0.05	0.05	0.06	0.03	0.13	0.06	0.01	0.10	0.08
K	0.30	0.19	0.17	0.21	0.20	0.18	0.12	0.10	0.16	0.18	0.34	0.35	0.15	0.11	0.11
Totals	0.37	0.25	0.23	0.39	0.31	0.20	0.19	0.18	0.24	0.23	0.53	0.42		0.22	
Fe/(Fe+Mg)	0.81	0.81	0.86	0.86	0.86	0.82	0.84	0.84	0.85	0.81	0.88	0.81	0.82	0.80	0.79

The least-altered BIF generally has higher SiO_2 contents (70.23±11.09 wt%) and lower Fe_2O_3 total (25.36± 10.28 wt%) than the altered samples, which have 40.13± 11.09 and 39.56±7.76 wt%, respectively, as major constituents—a feature that can be attributed to increasing carbonation and/or sulphidation in more altered samples. There is a lack of a close relationship between Au and the other pathfinder elements (Ag, Sb, As, W, Bi and Te) as indicated by very low correlation coefficients (r=0.14 for Au–Ag, r=0.22 for Au–Sb, r=0.12 for Au–As, r=0.22 for Au–W, r=0.44 for Au–Bi and r=0.23 for Au–Te).

Comparison of the composition of least-altered BIF samples at Kalahari Goldridge with major element compositions of other worldwide BIFs, as summarised in Klein (1983), indicates relatively high SiO_2 contents against a common range of up to 68 wt% in most worldwide BIFs. In isolated cases, higher SiO_2 ranging up to 88 wt% has been documented in some BIFs (e.g. 16.1 to 87.2 wt%, Klein 1978; 26.6–86.5 wt%, Lesher 1978; 6–88 wt%, Dymek and Klein 1988; 30.51–90.43 wt%, Manikyamba et al. 1993), with the high variability in SiO_2 in these samples reflecting variation in chert- or quartz-rich bands within the BIF. On the basis of Fe_2O_3total and SiO_2 as major constituents (e.g. Manikyamba et al. 1993), samples containing <15 wt% Fe_2O_3total are classified as ferruginous cherts, and samples containing >15 wt% Fe_2O_3—total are cherty BIF. Least-altered BIF at Kalahari Goldridge with average Fe_2O_3—total 28.93±10.28 wt% and 70.23±11.09 wt% for SiO_2 BIF may be classified as cherty BIF.

Alteration geochemistry

The study of hydrothermal alteration in lode-gold deposits based on the relative chemical variation in major and trace elements has been widely used (Ludden et al. 1984; Kishida and Kerrich 1987; Love and Roberts 1991; MacLean and Hoy 1991; Fleet et al. 1997; Eilu et al. 2001) in Archaean greenstone belts to determine the chemical composition of the mineralising fluid and history of the hydrothermal alteration, as well as to identify precursor rock types. Differences in the geochemical

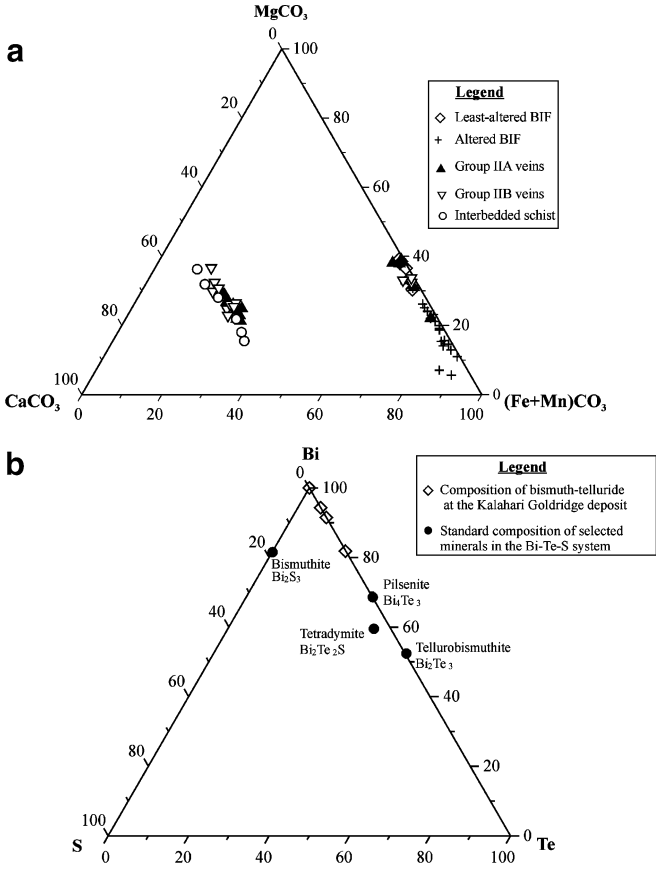

Fig. 7 **a** Ternary plot of compositions of carbonates (excluding calcite) occurring in the orebody at the Kalahari Goldridge deposit. **b** Ternary plot showing the compositional range of bismuth minerals (*open squares*) at the Kalahari Goldridge deposit in the Bi–Te–S system. Shown for reference are common bismuth minerals in the ternary system (Marcoux et al. 1996)

composition of the hydrothermally altered and unaltered lithologies are generally related to both mineralogical and bulk chemical changes, and are thus functions of mass changes. Examination of mass changes during hydrothermal alteration has been achieved by mass balance calculations using elements that are traditionally considered immobile, such as Al, Ti, high-field strength elements (HFSE), Zr, Nb and Y, and REE to monitor mass and volume changes during hydrothermal alteration (MacLean and Kranidiotis 1987; MacLean and Barrett 1993).

The method of Grant (1986) was used to determine chemical mass changes associated with metasomatism at Kalahari Goldridge. The quantitative relationship for the mass change (ΔC) is given as: $\Delta C\,(\%) = 100\left\{\left[M^A/M^O\left(C^A/C^O\right)\right]\right\} - 1)$, where M^O and M^A are the masses of rocks in an equal-sized rock volume of the parent and altered rocks, respectively, and C^A and C^O represent the element concentrations of the altered and original rocks, respectively. Elements that remained immobile during fluid–rock interaction plot on a line called an isocon, which defines a straight line through the origin given by $C^A = M^O/M^A C^O$, where the ratio M^O/M^A is equivalent to the slope of the straight line. A slope of one represents isovolumetric behavior. Components that lie above the isocon indicate enrichment in the altered rock, and depletion if they plot below the line.

Figure 10 illustrates plots for best-fit and constant volume isocons for Kalahari Goldridge. With the exception of the SiO_2, which plots below the constant volume isocon line, all the elements lie above this line, which implies addition to the system at constant volume. This suggests that traditionally considered 'immobile' elements such as Zr, Nb, Y, La, Ce and Al_2O_3 were several folds added during hydrothermal alteration—a situation which seems quite unrealistic. A best-fit line through the entire list of

Table 4 Representative microprobe analyses of gold and bismuth telluride grains

Sample	Bi minerals				Au									
	1		2		3		4		5		6		7	
No. of analyses	4		3		7		15		5		4		3	
	Mean	SD	Mean	SD	Mean	SD	Mean	SD	Mean	SD	Mean	SD	Mean	SD
Element														
Au	0.10	0.16	0.06	0.05	81.66	0.77	88.94	2.64	90.10	2.98	91.59	0.26	91.67	0.26
Ag	0.03	0.03	0.00	0.00	17.07	0.34	10.61	2.97	9.57	1.81	8.01	0.18	7.99	0.39
Cu	0.01	0.01	0.01	0.01	0.02	0.02	0.01	0.01	0.05	0.06	0.03	0.01	0.01	0.02
Fe	1.03	0.56	0.90	0.32	0.68	0.48	0.30	0.40	0.16	0.03	0.13	0.01	0.13	0.00
Bi	88.02	5.63	97.80	1.23	0.00	0.00	0.00	0.00	0.00	0.00	0.00	0.00	0.00	0.00
As	0.00	0.00	0.00	0.00	0.00	0.00	0.00	0.00	0.00	0.00	0.00	0.00	0.00	0.00
Te	10.66	6.53	0.00	0.00	0.02	0.02	0.00	0.00	0.00	0.00	0.00	0.00	0.03	0.01
S	0.05	0.09	0.34	0.50	0.07	0.08	0.14	0.02	0.08	0.07	0.14	0.01	0.08	0.08
Se	0.03	0.04	0.00	0.00	0.00	0.00	0.00	0.00	0.00	0.00	0.00	0.00	0.00	0.00
Total	99.91	1.12	99.10	0.89	99.51	0.91	100.01	0.33	99.93	1.15	99.89	0.05	99.90	0.04
Fineness					827	3	893	30	904	19	920	2	920	4

1, bismuth telluride; 2, native bismuth; 3, gold associated with bismuth minerals; 4, gold inclusions in pyrite; 5, gold-pyrrhotite inclusions in pyrite; 6, gold in pyrite fractures; 7, gold-carbonate inclusions in pyrite
SD one standard deviation

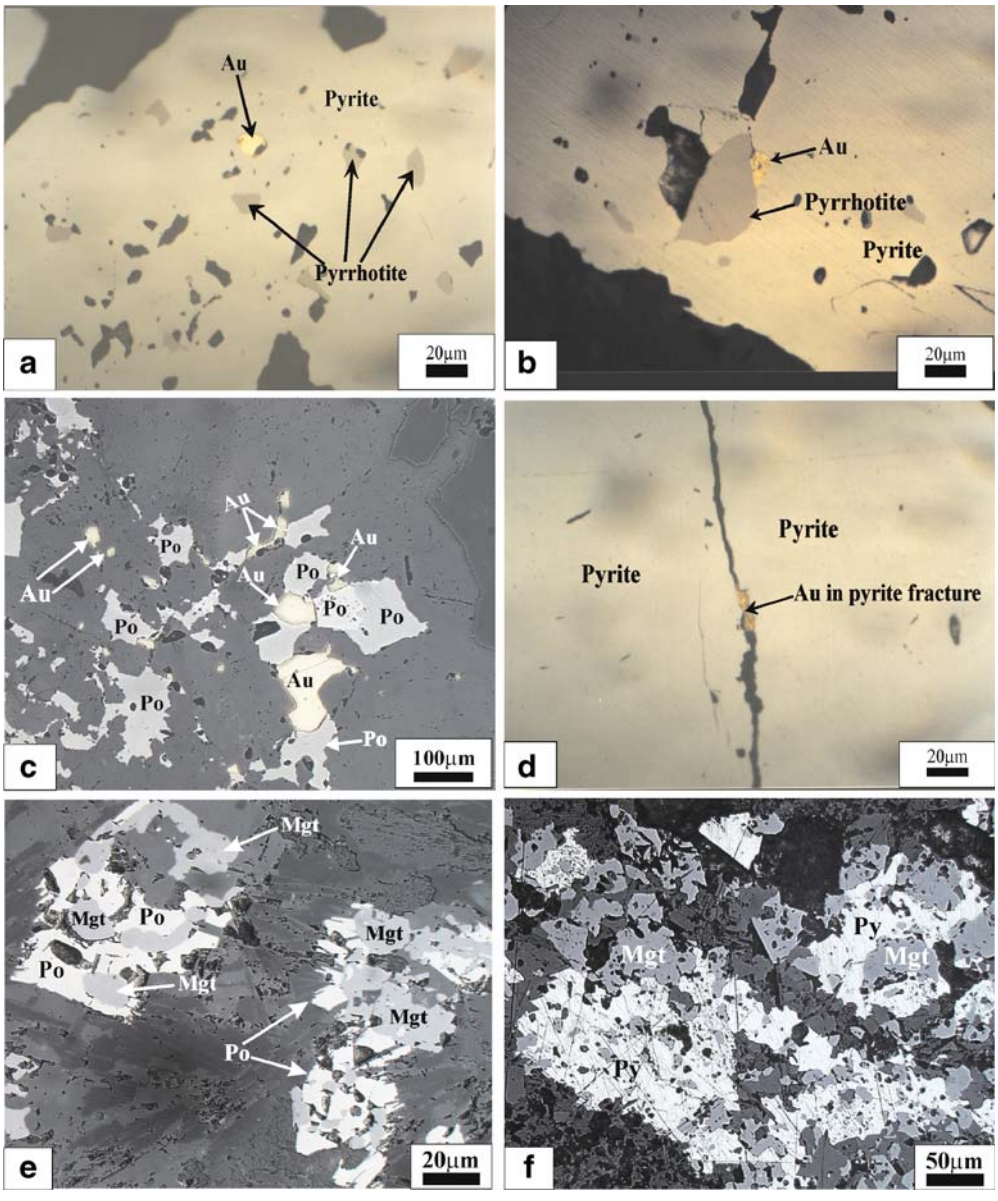

Fig. 8 Photomicrographs showing textural relationship among gold (Au), pyrite and pyrrhotite at the Kalahari Goldridge deposit: **a** Gold and pyrrhotite inclusions in pyrite; **b** gold–pyrrhotite inclusion in pyrite; **c** Gold association with pyrrhotite (Po); **d** gold in microfractures in pyrite; **e** replacement of magnetite (Mgt) by pyrrhotite (Po); **f** replacement of magnetite (Mgt) by pyrite (Py)

elements provides a more plausible isocon with a slope of approximately 2, representing about 50% volume loss. The best-fit isocon also passes through Al_2O_3, which suggests it was relatively immobile during hydrothermal alteration and, therefore, can be used to quantify the mass changes.

The mass change calculation based on constant Al_2O_3 shows significant depletion (75%) of SiO_2, while Fe (expressed as $Fe_2O_{3–Total}$) exhibited moderate depletion of about 40%, (Fig. 11a). The significant volume loss associated with the alteration can largely be attributed to loss of silica through leaching of the altered BIF, with possible re-precipitation in the adjacent extensional fractures in the quartz-carbonate veins. Leaching of silica is also consistent with the apparent enrichment of Al in the altered BIF, which is indicated by the presence of Al-bearing phyllosilicates such as stilpnomelane, chlorite and muscovite. Aluminium, however, may have been sourced locally from detrital components (e.g. aluminous clay minerals) by in situ enrichment given the paucity of Al in pristine BIFs.

Minor depletion of Fe may also be attributed to the deposition of Fe in the quartz veins mostly as sulphide minerals, carbonate minerals and chlorite, but the retention of a large proportion of Fe as sulphides and carbonates in the altered BIF. Metasomatic enrichment in MgO, MnO and CaO is attributed to carbonatisation, and also to chloritisation through that lead to Mg enrichment.

The transition elements Zn, Cu and Cr were largely immobile, whereas variable enrichment is indicated in Ni, V and Co (25, 45 and 105%, respectively). A strong enrichment in Sc is noted (average 557%, Fig. 11b). As

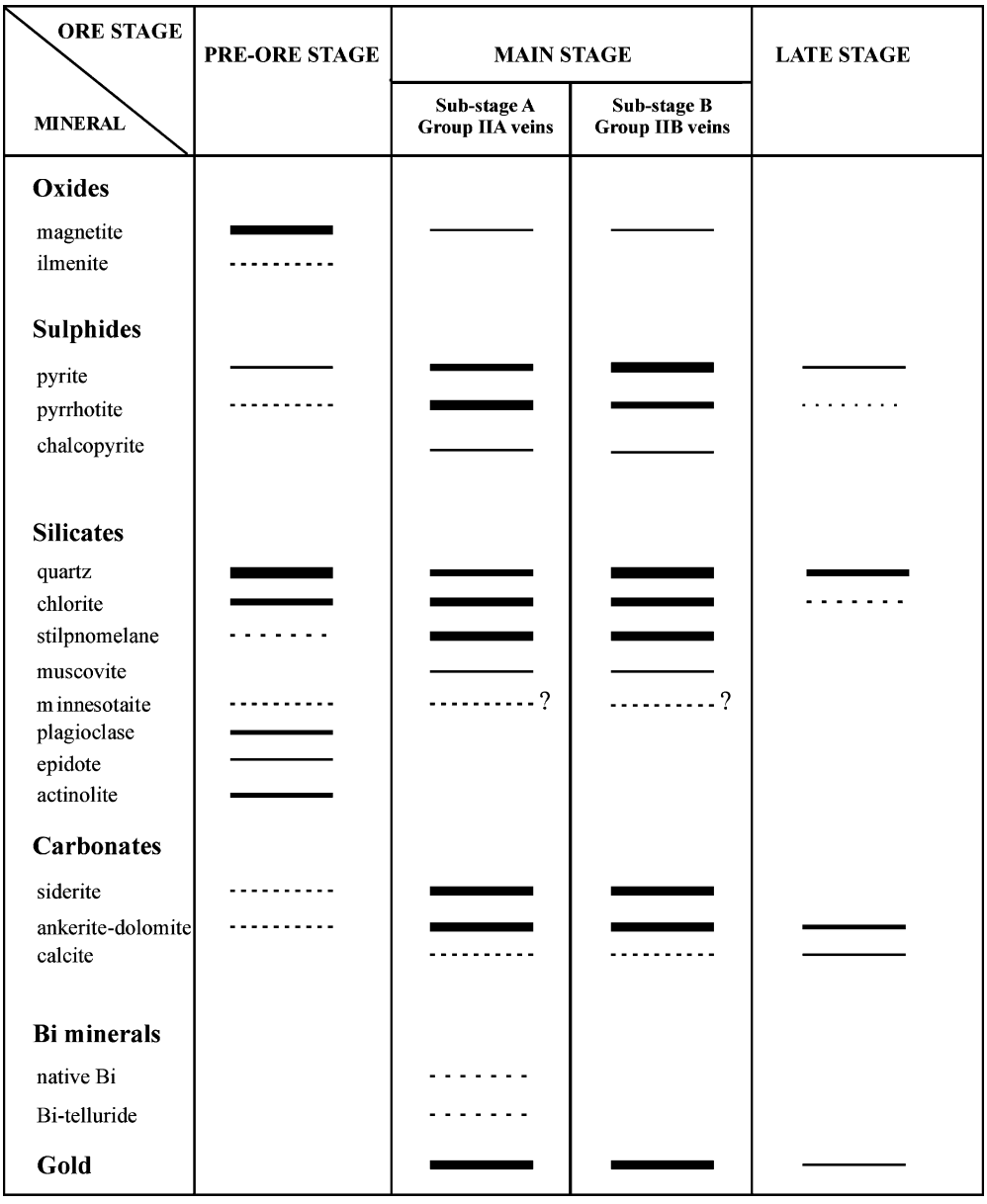

Fig. 9 Simplified paragenetic sequence for mineralisation at the Kalahari Goldridge deposit

expected from the mineral assemblage in the altered samples, the large ion lithophile elements, Ba, Sr, CaO, K_2O and Rb, show significant addition from the hydrothermal fluid (Fig. 11c). Enrichment in Sr (98%) can be ascribed to ankerite formation sympathetically with CaO, whereas that in Ba, Rb and K_2O, may be attributed to the extensive K-metasomatism, with these elements being incorporated into muscovite and stilpnomelane. The pathfinder elements and precious metals (Fig. 11d) are characterised by variable relative mass changes, with enrichment in Au (115%), Ag (92%) and As (171%), and depletion in Sb (57%) and W (60%), whereas Te was relative stable. The rare-earth elements Nd, Nb, Ce and La remained largely unchanged. However, the high field strength elements Zr and Y experienced some mobility, Zirconium enrichment reaching approximately 150%, whereas Y experienced a loss of 40%.

The mobility of the high-field strength elements Zr and Y during hydrothermal alteration at Kalahari Goldridge is consistent with the general observation that under certain conditions of hydrothermal alteration, light REE and HFSE can be mobile (MacLean and Barrett 1993). A number of studies (Ludden et al. 1984; Moritz and Crocket 1991; Eilu et al. 2001) have demonstrated the mobile behavior of these 'immobile' elements during alteration in some Archaean lode-gold deposits. In these studies, the mobile behavior of these elements is attributed to intense carbonatisation. This conclusion has been demonstrated by Langmuir (1979), who showed that in fluids containing high levels of CO_2, these 'immobile' elements, due to their high valency, favour the formation of stable carbonate complexes, and, hence, are readily transported in the hydrothermal fluid. The extensive carbonate alteration at the Kalahari Goldridge deposit can, thus, explain the significant mobility of Zr and Y.

Table 5 Mean and standard deviation (SD) for least-altered and altered BIF at the Kalahari Goldridge deposit

	Least-altered BIF		Altered BIF	
	Mean	SD	Mean	SD
	n=8		*n*=38	
In weight percent (wt%)				
SiO_2	70.23	11.12	40.13	11.13
TiO_2	0.02	0.00	0.05	0.05
Al_2O_3	0.24	0.36	0.53	0.52
Fe_2O_3–Total	25.36	10.17	39.56	7.76
MnO	0.21	0.13	0.74	0.20
MgO	0.76	0.61	3.10	0.77
CaO	0.77	0.49	2.88	1.60
Na_2O	0.01	0.04	0.04	0.04
K_2O	0.03	0.02	0.13	0.19
P_2O_5	0.11	0.09	0.18	0.13
LOI	2.54	1.68	12.38	3.36
Total	100.27	0.40	99.72	0.76
In parts per million (ppm)				
Zn	34.27	11.61	73.78	47.80
Cu	22.43	25.37	46.84	45.69
Ni	8.33	2.55	22.72	18.92
Co	1.88	0.96	8.40	7.65
Cr	12.49	1.83	27.11	19.68
V	4.77	2.13	15.44	10.40
Sc	0.10	0.13	1.47	1.31
Ce	4.91	2.22	9.61	5.01
Nd	2.71	1.30	5.33	2.88
La	2.46	1.12	4.62	2.23
Nb	0.12	0.06	0.24	0.25
Zr	0.86	0.97	4.73	3.23
Y	3.92	2.42	5.17	2.46
Ag	0.04	0.07	0.16	0.13
Sb	0.33	0.16	0.30	0.24
As	1.11	0.68	6.55	13.85
W	0.94	0.29	0.79	0.37
Bi	1.87	3.42	6.78	6.28
Te	0.13	0.21	0.29	0.51
Au	0.02	0.04	0.11	0.11
Ba	7.24	4.83	45.58	40.34
Sr	10.00	6.34	43.17	31.01
Rb	1.17	0.86	6.08	6.79

Discussion and conclusions

Mineralogical characteristics

Metamorphic mineral assemblage

Studies reported in the literature on the metamorphic grades of BIFs hosting gold deposits (Saager et al. 1987; Pretorius et al. 1988; Lhotka and Nesbitt 1989; Vielreicher et al. 1994) indicate a range from low- to medium-grade metamorphism. In general, at the lowest metamorphic grades, BIF is commonly characterised by quartz-magnetite–minnesotaite-stilpnomelane-greenalite-siderite assemblages, which grade up to quartz-magnetite-grunerite± stilpnomelane±minnesotaite-siderite assemblages in low-amphibolite facies grades (Gole 1980; Klein 1974, 1983; Miyano and Klein 1989). In particular, several studies (e.g. James 1955; French 1973; Klein and Flink 1976; Miyano 1982; Miyano and Klein 1989) have documented the stability limits for minnesotaite to range from 275° to 400°C, where minnesotaite converts to grunerite. The presence of minnesotaite and absence of grunerite in least-altered BIF at Kalahari Goldridge, therefore, provides a basic constraint on the maximum temperature (~400°C) of metamorphism of the BIF before mineralisation. Its complete absence in the altered BIF may be attributed to thermal instability due to higher temperature gradients during mineralisation.

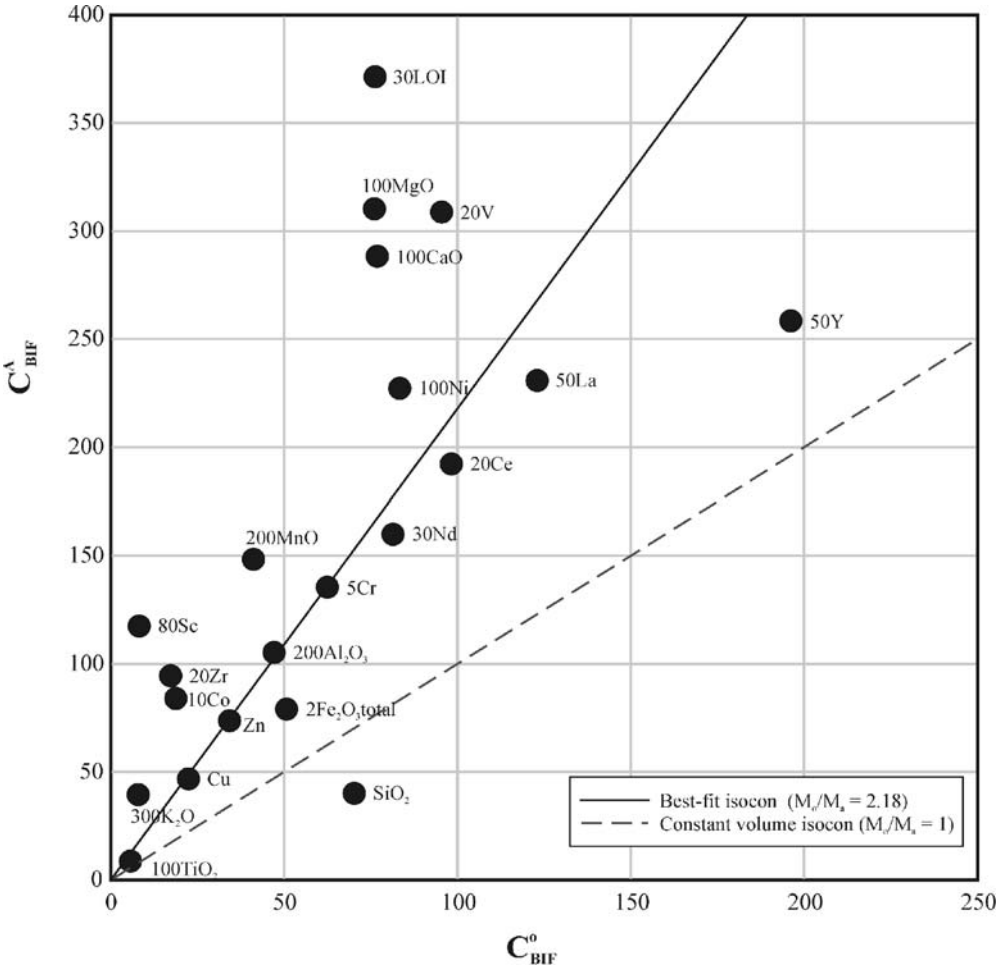

Fig. 10 Isocon diagram for average least-altered and altered BIF at Kalahari Goldridge Mine. Best-fit and constant volume isocons are plotted following the method of Grant (1986) to determine mass changes associated with alteration at the Kalahari Goldridge deposit

Gold fineness

High-average gold values and restricted fineness range (890–960) are characteristic of Archaean lode deposits (Morrison et al. 1991). In BIF-hosted deposits, fineness ranging from 851 to 970 has been previously reported (Saager et al. 1987; Pretorius et al. 1988; Vielreicher et al. 1994). The high fineness of gold in Archaean systems has been attributed to sulphidation associated with gold deposition (Morrison et al. 1991). The Au–Ag ratio of electrum in equilibrium with fluid has been demonstrated to be a function of Cl^-/H_2S ratio, pH, and Au/Ag ratio in the fluid (Morrison et al. 1991; Gammons and Williams Jones 1995). These authors demonstrated that H_2S-rich fluids or increased a_{SO4}/a_{H2S} ratio in the hydrothermal fluid favours the precipitation of Au, whereas Ag is favoured by $AgCl^-$. Morrison et al. (1991) also associated the consistency in the fineness of gold in Archaean terranes to three possible reasons: (1) a unique origin for the style of mineralization; (2) unique source of the gold; and (3) a mechanism of homogenising the fineness values through post-mineralisation metamorphism. Anhaeusser (1986) stated that consistency of gold fineness in general is characteristic of gold that precipitated in a single stage in the paragenesis of the ore. Higher temperature deposits also show greater abundances of Ag than lower temperature deposits (Marcoux et al. 1996). Therefore, the close association of the bismuth minerals with pyrrhotite (which precipitates at low a_{H_2S}) and the lower fineness in gold (higher Ag) associated with the bismuth minerals suggests that their precipitation occurred at higher temperatures.

Fe/(Fe+Mg) ratio and fO2 variation in chlorite

High Fe/(Fe+Mg) ratios in chlorite from BIF compared to that from the interbedded schist (Table 2) closely reflect host rock composition, and, to a lesser extent, alteration. However, the variation in vein chlorite composition can be attributed to changes in oxygen fugacity (fO_2) and/or sulphur fugacity (fS_2).

At a given temperature and pressure, Bryndzia and Scott (1987) showed that Fe/ (Fe+Mg) ratios in chlorite can vary as a result of sulphidation and oxidation processes. In particular, Fe/(Fe+Mg) ratios in chlorite decrease with increasing fO_2 in the magnetite stability field, increasing fO_2 and fS_2 in the coexisting magnetite–pyrrhotite stability field, or increasing fS_2 in the pyrrhotite stability field. Given that group IIA veins are generally more pyrrhotite-rich than the group IIB veins at Kalahari Goldridge, the lower Fe/(Fe+Mg) ratios of chlorite from group IIB veins

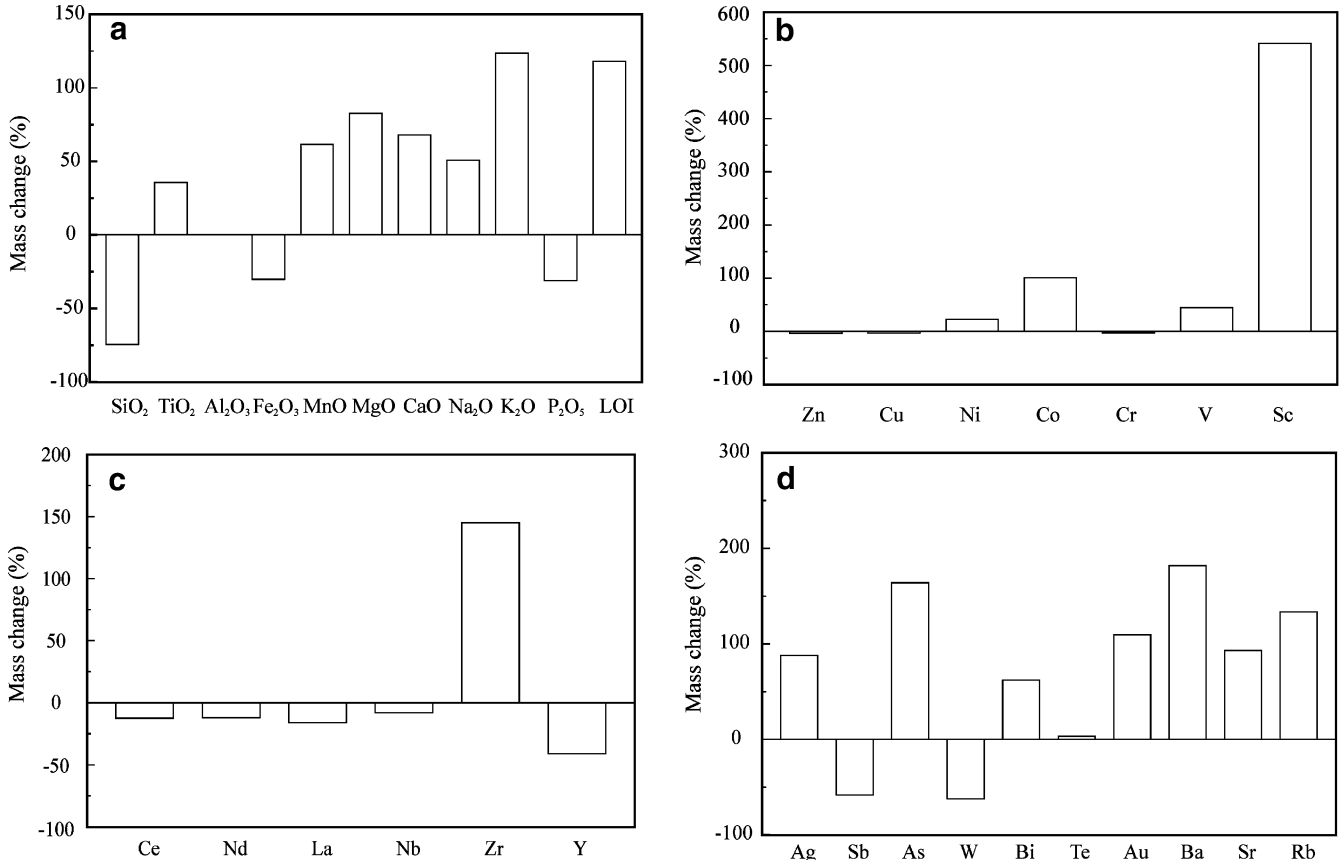

Fig. 11 Mass changes of major and trace elements during hydrothermal alteration at the Kalahari Goldridge Mine. Gains and losses are expressed in percentage relative to least-altered samples using the approach of Grant (1986)

relative to group IIA veins are consistent with increase in fO_2 and/fS_2 during vein formation as indicated by the sulphide assemblages.

Controls on mineralisation

Gold mineralisation at the Kalahari Goldridge deposit is interpreted to be controlled by three main factors: contrast in competency, geochemistry of host rock and structure.

Significance of competency contrast

Although the distribution of high gold grades at the Kalahari Goldridge deposit is somewhat irregular, the most economically viable part of the ore body is associated with the most competent and Fe-rich part of the stratigraphy, which consists of the BIF unit (Figs. 12a and 13). A large proportion of the gently dipping ladder veins (group IIA) are confined to the BIF units, which indicates that high fluid pressure played an important role in fluid infiltration and gold mineralisation. The associated fracturing and shearing provided conduits for infiltration of ore fluids and outlines the importance of host-rock competence and fluid focusing in ore deposition. Although the interlayered schists are less mineralised, foliation planes in these metasedimentary rocks as well as lithological discontinuities between BIF and these units are also likely to have served as conduits for upward-migrating ore fluids. In places, this is indicated by the complete replacement of narrow magnetite mesobands, interlayered within the schist, by pyrrhotite. The boudins and tight isoclinal folds in the cherty BIF, as well as sigmoidal veins, are characteristic of ductile deformation. However, the selective extension veins in Fe-rich layers in the BIF indicate that more brittle deformation was locally dominant, and that mineralisation at the Kalahari Goldridge deposit occurred under conditions of brittle–ductile deformation.

Influence of chemical composition of host rock

Sulphidation haloes associated with the large gently dipping veins (group IIB) are generally confined to the BIF, even though the veins may cut across the BIF into the footwall and hanging wall units. Ore shoots are characterised by sulphide haloes on both sides of crosscutting gently dipping extension veins into favourable BIF layers. Consistently high gold grades are associated with sulphide and carbonate alteration zones in the BIF rather than with veins. This suggests that the relatively high Fe/Fe+Mg ratio of the BIF influenced the distribution and localisation of gold deposition through desulphidation of the fluid at

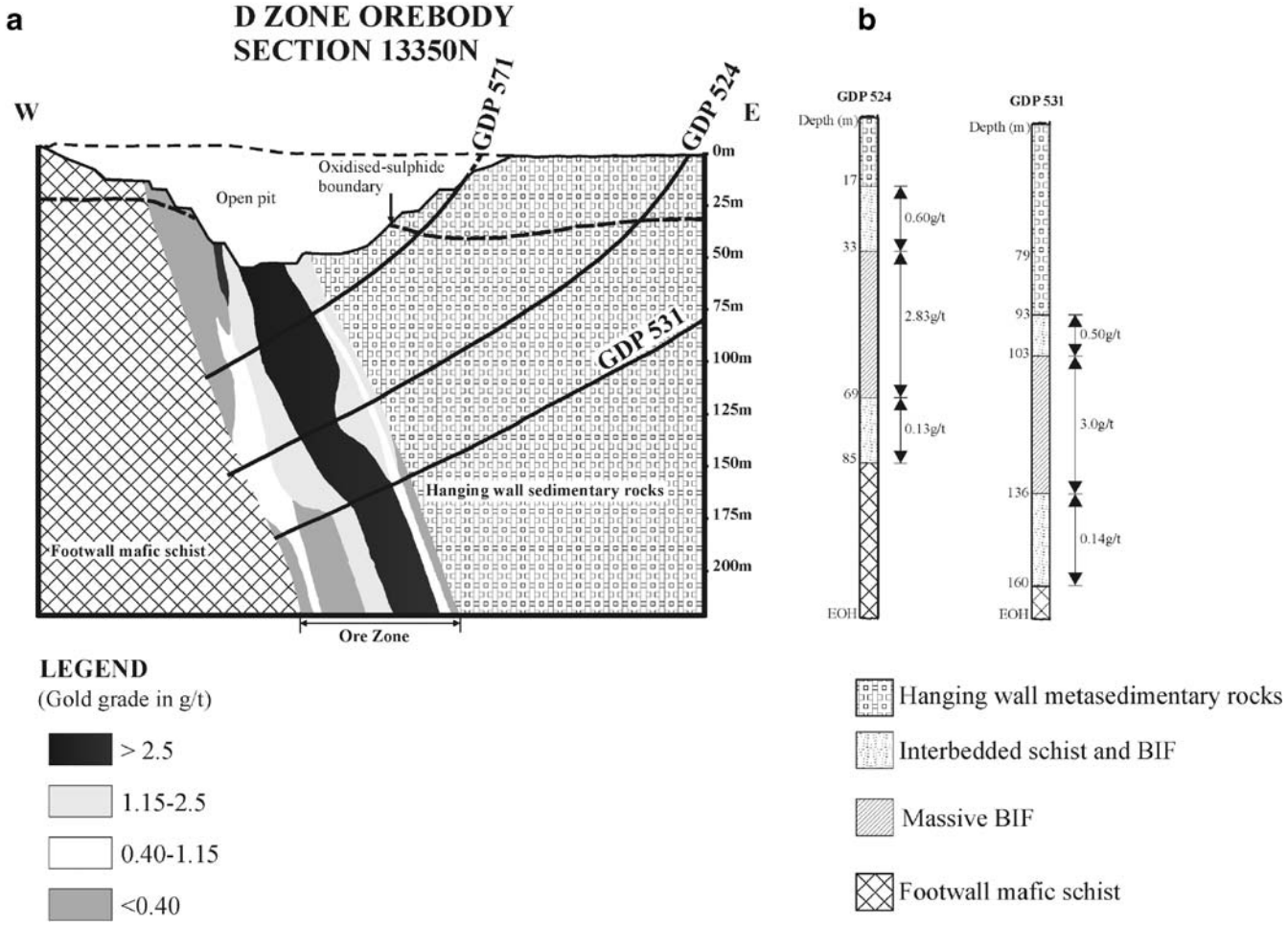

Fig. 12 **a** Distribution of gold mineralisation in the D-zone orebody, Kalahari Goldridge deposit. Highest gold grade occurs in massive BIF located centrally in the orebody (figure redrawn from Kalahari Goldridge Mine annual report, 1998). **b** Simplified section through borehole intersections GDP 524 and GDP 531 showing average gold grades in lithologies in the orebody. *EOH* End of hole

Kalahari Goldridge (Fig. 12a and b). Locally, high gold grades are associated with carbonaceous phyllites at contacts between the footwall and the BIF horizon, suggesting that gold deposition may also have been related to fluid reaction with carbon-bearing metasedimentary rocks.

Structural control

The distribution of gold mineralisation at Kalahari Goldridge is controlled by structures developed within favourable rocks during folding and deformation. The fold geometry and orientation of mineral-elongation lineations in the BIF provide major controls on the localisation of gold mineralisation.

The ladder veins (group IIA) are orthogonal to the axial planes of the isoclinal folds, due to extension related to folding, and, therefore, their distribution is controlled by the plunge of the fold axes. As expected, the major ore shoots enveloping the group IIA ladder veins have a plunge of approximately 80° E. In contrast, the group IIB veins are not closely related to early folding, and, therefore, related ore shoots plunge along the intersection of the veins with the major reactive BIF unit. They, therefore, plunge to the north at approximately 341°/08° N (Fig. 5c), overprinting the earlier-formed ore shoots. These structural features that control the ore shoots are characteristic of many Archaean lode-gold deposits documented in the literature (e.g. Hodgson and Hamilton 1989; Peters 1993; Vearncombe 1993).

Timing of gold mineralisation

The gently dipping extensional vein systems (group IIA) at the Goldridge deposit, which clearly transect the regional metamorphic foliation, postdated or are late with respect to the regional metamorphism which occurred during D_1. The post-metamorphic nature of the mineralisation is also documented in the interbedded schist where alteration-related muscovite + stilpnomelane have replaced foliation-parallel metamorphic chlorite.

The relationship between the alteration assemblage, gently dipping (groups IIA and IIB) veins and isoclinal structures places the main mineralisation event within D_2 deformation, which controlled the geometry of the lode

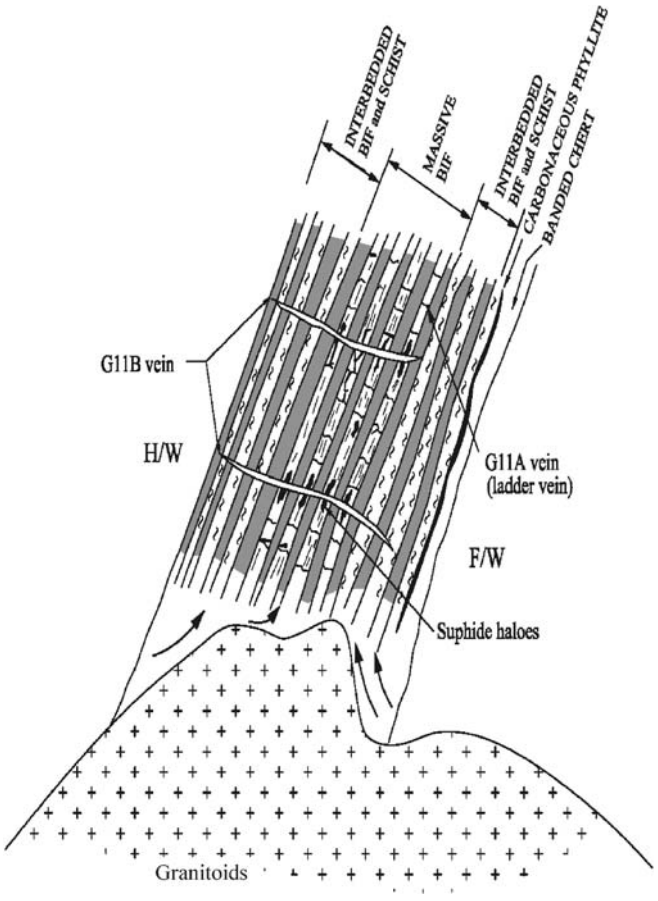

Fig. 13 Simplified schematic diagram showing ore fluid path and associated sulphide alteration haloes at the Kalahari Goldridge deposit. *H/W* Hanging wall, *F/W* footwall

system. The localisation of gold mineralisation in more competent BIF and its association with crosscutting gently dipping veins indicate that mineralisation was superimposed on the Fe-rich lithology. The absence of chlorite in the least altered BIFs, but its dominance in altered samples in association with coarse-grained stilpnomelane and other alteration minerals, indicates that mineralisation was contemporaneous with hydrothermal alteration. Vein growth, which commenced with group IIA veins followed by the group IIB veins, probably occurred over an extended period but during a single progressive deformation. Mineralisation occurred within a uniform stress regime, as demonstrated by similar structural orientation of the two vein types (IIA and IIB) related to gold mineralisation.

Genetic model

BIF-hosted gold mineralisation forms an integral part of many Archaean greenstone belts in countries such as Australia (e.g. Mt. Morgans; Vielreicher et al. 1994), Brazil (Morro Velho; Ladeira 1991), Canada (Lupin; Lhotka and Nesbitt 1989), South Africa (Fumani; Pretorius et al. 1988) and Zimbabwe (Vubachikwe; Saager et al. 1987). The varying styles of gold mineralisation in BIF have led to the proposition of three different genetic models, namely, syngenetic, epigenetic and a hybrid of both the epigenetic and syngenetic (multistage) models for its deposition (Fripp 1976; Phillips et al. 1984; Groves et al. 1987; Saager et al. 1987; Ladeira 1991) The syngenetic model proposes that sulphide minerals, carbonate minerals, chert and gold were deposited from the hydrothermal fluids on the seafloor during chemical sedimentation (e.g. Vubachikwe, Fripp 1976; Morro Velho, Ladeira 1991).

Evaluation of textural relationships, geochemical data and structural information at the Kalahari Goldridge deposit indicate that gold mineralisation postdates chemical sedimentation of the ferruginous host rock and is epigenetic. Furthermore, the low base-metal content associated with the sulphide mineralogy renders possible submarine volcanic activity for the genesis of gold at Kalahari Goldridge unlikely (Kerrich and Fryer 1979). Further support for an epigenetic origin includes: (1) close association with hydrothermal alteration and quartz–carbonate extension veins, which crosscut lithological layering of the host BIF; (2) meso- and micro-scale discordant replacement of foliation-parallel magnetite by pyrite, pyrrhotite and siderite along vein margins; (3) close association of gold with sulphide/carbonate-rich layers formed by replacement of oxide-facies BIF adjacent to transgressive quartz-carbonate veins; and (4) absence or minimal occurrence of sulphides and carbonate as well as low Au tenors in least-altered BIF samples. Fluid interaction with host rock along fluid conduits clearly resulted in selective replacement of iron oxides and iron silicate mineral by sulphide and carbonate minerals.

Exploration significance

In most gold terranes, conventional geochemical methods have commonly been used for exploring concealed deposits. In this method, coherent correlation between Au and normally gold-associated elements such as As, Bi, W, Te, Sb and Se has proved useful in targeting concealed deposits. At the Kalahari Goldridge deposit, the current study has revealed no coherent correlations between Au and these elements and, therefore, casts doubt on the use of conventional pathfinder elements as an exploration tool. However, despite this lack of coherent correlation, the mass balance calculation shows that an increase in Au is accompanied by co-enrichment in some major (K, Mg and Na) and trace elements (As, Te, Bi, and Ag, Rb, Ba, Zr and Sc), which suggests that all trace elements that show anomalous enrichment (As, Te, Bi, Ag, Rb, Ba, Zr, Sc and K) with Au at Kalahari Goldridge should be used as pathfinders in the BIFs. In particular, extremely high enrichment in Sc, although present at low levels 0.1± 0.13 and 1.47±1.31 ppm for the least-altered and altered BIF, respectively, may serve as an important geochemical tool for exploration in ferruginous sedimentary rocks in the Kraaipan region.

Acknowledgements This paper forms part of NQH'S Ph.D. thesis. Financial support was provided by the Kalahari Goldridge Mine to NQH and the National Research Foundation, South Africa to JMM. Special thanks go to the Society of Economic Geologists Foundation for a Hugh E. McKinstry student research grant awarded to NQH. We express our appreciation to T. Miyano of the Institute of Geosciences, University of Tsukuba for discussions on stilpnomelane and minnesotaite in BIF and F. Dabrowski, D. Grobler and P. Hilliard of Kalahari Goldridge/Harmony for assistance and support at the mine. Discussions with P. Hilliard provided significant insight into the structural geology of the deposit. The 1998/1999 Rhodes University MSc students are thanked for their assistance with the collection of structural data. We wish to express our sincere appreciation to D. I. Groves, C. R. Anhaeusser and Hartwig Frimmel whose critical reviews greatly improved this manuscript.

References

Anhaeusser CR (1986) Archaean gold mineralization in the Barberton Mountain land. In: Anhaeusser CR, Maske S (eds) Mineral deposits of Southern Africa. Geological Society of South Africa, pp 113–154

Anhaeusser CR, Walraven F (1999) Episodic granitoid emplacement in western Kaapvaal Craton: evidence from the Achaean Kraaipan granite-greenstone terrane, South Africa. J Afr Earth Sci 28:289–309

Bryndzia LT, Scott SD (1987) Application of chlorite–sulfide–oxide equilibria to metamorphosed massive sulfide ores, Snow Lake area, Manitoba. Econ Geol 82:963–970

Burger AJ, Walraven F (1979) Summary of age determinations carried out the period from April 1977 to March (1978). Annals of Geological Survey of South Africa 12:209–218

Dymek RF, Klein C (1988) Chemistry, petrology and origin of banded iron-formation lithologies from the 3,800 Ma Isua supracrustal belt, West Greenland. Precambrian Res 39:247–302

Eilu P, Mikucki EJ, Dugdale AL (2001) Alteration zoning and primary geochemical dispersion at Bronzewing lode-gold deposit, Western Australia. Miner Depos 36:13–31

Fleet ME, Seller MH, Pan Y (1997) Rare earth elements, protolith, and alteration at the Hemlo gold deposit, Ontario, Canada, and comparison with argillic and serite alteration in the Highland Valley Porphyry district, British Columbia, Canada. Econ Geol 92:551–568

French BM (1973) Mineral assemblages on diagenetic and low grade metamorphic iron-formation. Econ Geol 168:1063–1074

Fripp REP (1976) Stratabound gold deposits in Archean banded iron-formation, Rhodesia. Econ Geol 71:58–75

Gammons CH, Williams-Jones AE (1995) Hydrothermal geochemistry of electrum: thermodynamic constraints. Econ Geol 90:420–432

Gole MJ (1980) Mineralogy and petrology of very low-grade metamorphic Archean banded iron-formations, Weld Range, Western Australia. Am Mineral 65:8–25

Grant JA (1986) The isocon diagram: a simple solution to Gresen's equation for metasomatic alteration. Econ Geol 81:1976–1982

Groves DI, Phillips GN, Falconer LJ, Houstoun SM, Ho SE, Browning P, Dahl N, McNaughton NJ (1987) Evidence for an epigenetic origin for BIF-hosted gold deposits in greenstone belts of the Yilgan block, Western Australia: In: Ho SE, Groves DI (eds) Recent advances in understanding Precambrian gold deposits. Geology Department and University Extension, The University of Western Australia Publication 11, pp 167–179

Hey MH (1954) A new review of the chlorites. Mineral Mag 30:277

Hodgson CJ, Hamilton JV (1989) Gold mineralization in the Abitibi Greenstone Belt: end-stage result of Achaean collisional tectonics. Econ Geol Monogr 6:86–100

James HL (1955) Sedimentary facies in iron-formation. Econ Geol 68:235–293

Jones IM, Anhaeusser CR (1993) Accretionary lapilli associated with Achaean banded iron formations of the Kraaipan Group, Amalia greenstone belt, South Africa. Precambrian Res 61:117–136

Kerrich R, Fryer BJ (1979) Archaean precious metal hydrothermal systems, Dome Mine, Abitibi greenstone belt. Can J Earth Sci 16:440–458

Kishida A, Kerrich R (1987) Hydrothermal alteration zoning and gold mineralization at the Kerr Addison Archean lode gold deposit, Kirkland Lake, Ontario. Econ Geol 82:649–690

Klein C (1974) Greenalite, stilpnomelane, minnesotaite, crocidolite and carbonates in a very low-grade metamorphic Precambrian iron-formation. Can J Earth Sci 12:475–498

Klein C (1978) Regional metamorphism of the Proterozoic iron-formation, Labrador Trough, Canada. Am Mineral 63:898–912

Klein C (1983) Diagenesis and metamorphism of Precambrian banded iron-formation. In: Trendall AF, Morris RC (eds) Iron formations: facts and problems. Elsevier, Amsterdam, pp 417–469

Klein C, Fink RP (1976) Petrology of the Sokoman Iron Formation of the Howells River area, at the western edge of the Labrador Trough. Econ Geol 71:453–488

Ladeira EA (1991) Genesis of gold in the Quadril'tero Ferrifero: a remarkable case of permanency, recycling and inheritance, a tribute to Djalma, Guimaraes, Pierre Routhier and Hans Ramsberg. In: Ladeira EA (ed) Gold '91. Balkama Publications, Rotterdam, pp 11–30

Langmuir D (1979) Techniques of estimating thermodynamic properties for aqueous complexes of geochemical interest. In: Jenne EA (ed) Chemical modelling—speciation, sorption, solubility and kinetics in aqueous systems. Proceedings of American Chemical Society Symposium, vol. 93. Washington DC, pp 353–387

Lesher C (1978) Mineralogy and petrology of the Sokoman Iron-formation near Ardua Lake, Quebec. Can J Earth Sci 15:480–500

Lhotka PG, Nesbitt BE (1989) Geology of unmineralized and gold-bearing iron-formation, Contwoyto Lake Point Lake region, Northwest Territories, Canada. Can J Earth Sci 26:46–64

Love DA, Roberts RG (1991) The geology and geochemistry of gold mineralization and associated alteration at the Rundle gold deposit, Abitibi Subprovince, Ontario geochemistry of altered rocks at the Horne mine, Noranda, Quebec. Econ Geol 86:506–528

Ludden JN, Daigneault R, Robert F, Taylor RP (1984) Trace element mobility in alteration zones associated with Achaean Au lode deposits. Econ Geol 79:1131–1141

MacLean WH, Barrett TJ (1993) Lithogeochemical techniques using immobile elements. J Geochem Explor 48:109–133

MacLean WH, Hoy LD (1991) Geochemistry of altered rocks at the Horne mine, Noranda, Quebec. Econ Geol 86:506–528

MacLean WH, Kranidiotis P (1987) Immobile elements as monitors of mass transfer in hydrothermal alteration: Phelps Dodge massive sulfide deposit, Matagami, Quebec. Econ Geol 82:951–962

Manikyamba C, Balaram V, Naqvi SM (1993) Geochemical signatures of polygenetic origin of a banded iron-formation (BIF) of the Achaean Sandur greenstone belt (schist belt) Karnataka nucleus, India. Precambrian Res 61:137–164

Marcoux E, Moelo Y, Leistel JM (1996) Bismuth and cobalt minerals as indicators of stringer zones to massive sulfide deposits, Iberian Pyrite Belt. Miner Depos 31:1–26

Miyano T (1982) Stilpnomelane, Fe-rich mica, K-feldspar and hornblende in iron-formation assemblages of the Dales Gorge Member, Hamersley Group, Western Australia. Can Miner 20:189–202

Miyano T, Klein C (1989) Phase equilibria in the system K_2O–FeO–MgO–Al_2O_3–SiO_2–H_2O–CO_2 and the stability limit of stilpnomelane in metamorphosed Precambrian iron-formations. Contrib Mineral Petrol 102:478–491

Moritz RP, Crocket JH (1991) Hydrothermal wall-rock alteration of the gold-bearing quartz-fuchsite vein at the Dome mine, Timmins Area, Ontario, Canada. Econ Geol 86:620–641

Morrison GW, Jose WJ, Jaireth S (1991) Geological and geochemical controls on the silver content (fineness) of gold in gold–silver deposits. Ore Geol Rev 6:333–364

Norrish K, Hutton JT (1969) An accurate X-ray spectrographic method for the analysis of a wide range of geological samples. Geochim Cosmochim Acta 33(4):431–453

Peters SG (1993) Nomenclature, concepts, and classification of oreshoots in vein deposits. Ore Geol Rev 8:3–22

Phillips GN, Groves DI, Martyn JE (1984) An epigenetic origin for Archean banded iron-formation-hosted gold deposits. Econ Geol 79:162–171

Poujol M, Anhaeusser CR, Armstrong RA (2002) Episodic granitoid emplacement in the Archaean Amalia–Kraaipan terrane, South Africa: confirmation from single zircon U–Pb geochronology. J Afr Earth Sci 35:47–161

Pretorius AI, van Reenen DD, Barton JM Jr (1988) BIF-hosted gold mineralization at the Fumani Mine, Sutherland greenstone belt, South Africa. S Afr J Geol 91:429–438

Saager R, Oberthür T, Tomschi H (1987) Geochemistry and mineralogy of banded iron-formation-hosted gold mineralization in the Gwanda Greenstone Belt, Zimbabwe. Econ Geol 82:2017–2032

SACS (South African Committee for Stratigraphy) (1980) Stratigraphy of South Africa. Part I. (Compiler, L. E Kent) Lithostratigraphy of the Republic of South Africa, South West Africa/Namibia, and the Republics of Bophuthatswana, Transkei and Venda: handbook, geological survey of South Africa, vol 8, p 690

Vielreicher RM, Groves DI, Ridley NJ, McNaughton NJ (1994) A replacement origin for the BIF-hosted gold deposit at Mt. Morgans, Yilgarn Block, W.A. Ore Geol Rev 9:325–347

Vearncombe JR (1993) Quartz vein morphology and implications for formation depth and classification of Archaean gold-vein deposits. Ore Geol Rev 8:407–424

Zimmermann OT, Anhaeusser CR (1991) The northern Kraaipan granite-greenstone terrane. In: Anhaeusser CR (ed) The Achaean Kraaipan Group volcano-sedimentary rocks and associated granites and gneisses of the southwestern Transvaal, Northern Cape Province and Bophuthatswana. Information Circular, Economic Geology Research Unit, University of Witwatersrand, vol. 244, pp 26–28